Technical Report

TR-10-29

Damage tolerance analysis of canister inserts for spent nuclear fuel in the case of an earthquake induced rock shear load

Peter Dillström, Tobias Bolinder
Inspecta Technology AB

October 2010

Svensk Kärnbränslehantering AB
Swedish Nuclear Fuel
and Waste Management Co

Box 250, SE-101 24 Stockholm
Phone +46 8 459 84 00

ISSN 1404-0344
SKB TR-10-29

Damage tolerance analysis of canister inserts for spent nuclear fuel in the case of an earthquake induced rock shear load

Peter Dillström, Tobias Bolinder
Inspecta Technology AB

October 2010

Keywords: SKBdoc 1205067, Canister insert, Damage tolerance analysis, Shear load.

Contents

1 Introduction 5

2 FE analysis 7
2.1 Global FE-model 7
2.1.1 Boundary conditions, loading and material 7
2.1.2 Results for the global models 9
2.2 Submodels at the location with max principal stress 10
2.2.1 FE-models of surface defects 11
2.2.2 FE-models of internal defects 14
2.2.3 Results at the location with max principal stress component 15

3 Assumptions in the damage tolerance analysis 17
3.1 Insert geometry and postulated defects 17
3.2 Material properties – fracture toughness 17
3.3 Failure criteria and safety margins 19

4 Damage tolerance analysis at the location with max principal stress 21
4.1 Accepted defect size for internal defects 21
4.2 Accepted defect size for surface defects 23

5 Sensitivity study 25
5.1 Influence of bentonite clay density 25
5.2 Comparison between different defect geometry assumptions 26

6 Summary and conclusions 29

7 References 31

Appendix A Calculated ***J***-values when using a bentonite density of 1,950 kg/m^3 33

Appendix B Calculated ***J***-values when using a bentonite density of 2,000 kg/m^3 39

Appendix C Calculated ***J***-values when using a bentonite density of 2,050 kg/m^3 45

1 Introduction

Nuclear waste in Sweden is handled by the Swedish Nuclear Fuel and Waste Management Co, SKB. In the deep repository, copper canisters with a cast iron insert containing spent nuclear fuel are surrounded by bentonite clay and deposited at approximately 400 m depth in saturated, granitic rock.

The canisters consist of a pressure-bearing insert of nodular cast iron with a steel lid, Figure 1-1. The insert contains channels for the fuel assemblies, 12 in the BWR version and 4 in the PWR version. The insert is surrounded by an outer corrosion barrier of copper.

In the repository the canisters will be loaded in compression by the hydrostatic pressure and the swelling pressure from the surrounding bentonite. During the extreme time scales, several ice ages are expected with a resulting maximum ice-sheet of 3 km. The design pressure for the canisters has been set to be 45 Mpa /SKB 2009/. A damage tolerance analysis of the insert, using pressure loads, has been presented in /Dillström et al. 2010/.

During melting of the ice, there is also the possibility of an earthquake induced rock shear through a deposition hole. The effect on the canister by such a shear load has been investigated in /Hernelind 2010/. SKB has asked Inspecta Technology AB to perform a complementary damage tolerance analysis of the BWR cast iron insert. This report contains results of fracture mechanics analyses of the BWR insert with postulated defects. The aim of the analyses is to calculate acceptable defect sizes with regard to safety margins against fracture.

Figure 1-1. *Canister for final depository of spent nuclear fuel.*

2 FE analysis

The analyses of the BWR canister are conducted with the FE program ABAQUS /ABAQUS 2008/. A submodelling technique is used to introduce different defects in the BWR canister. When using a submodelling technique, a global model is used to retain the stresses and displacements of the canister. From these global results, the areas of interest are identified. In these areas the submodels containing the defects are introduced. The deformations from the global model are applied at the boundary of the submodel. From the submodel the *J*-integral results are then obtained. In the analyses three different setups of the global model are used and four different kinds of defects with three different crack depths are introduced using a submodelling technique. A total of 36 submodels are analyzed. Below is a summary of the examined cases.

Global models (equivalent to a rock shear perpendicular to the axis of the canister, hitting the canister at ¾ of the height from the bottom /Hernelind 2010/):

- Model6g_normal_quarter_1950ca3 (Bentonite density 1,950 kg/m^3).
- Model6g_normal_quarter_2000ca3 (Bentonite density 2,000 kg/m^3).
- Model6g_normal_quarter_2050ca3 (Bentonite density 2,050 kg/m^3).

Submodels:

- Semi-elliptical surface crack with a crack depth a = 1 mm, 5 mm, 10 mm and a crack length $2c = 6a$ = 6 mm, 30 mm, 60 mm.
- Semi-circular surface crack with a crack depth a = 1 mm, 5 mm, 10 mm and a crack length $2c = 2a$ = 2 mm, 10 mm, 20 mm.
- Elliptical internal crack with a crack depth $2a$ = 1 mm, 5 mm, 10 mm and a crack length $2c = 12a$ = 6 mm, 30 mm, 60 mm.
- Circular internal crack with a crack depth $2a$ = 1 mm, 5 mm, 10 mm and a crack length $2c = 2a$ = 1 mm, 5 mm, 10 mm.

The crack depth parameter a and the crack length parameter c is defined in Figure 2-5 (surface cracks) and Figure 2-11 (internal cracks).

2.1 Global FE-model

The global FE-model obtained from /Hernelind 2010/ is made up by 8 node brick elements (C3D8) and 8 node brick elements with reduced integration (C3D8R). Contact is defined between the copper shell and the cast iron insert. The channel tubes are assumed to be an integral part with the insert and therefore contribute as added material to the insert (this will probably overestimate the insert stresses and strains in this region). Only half the canister is modelled by using symmetry. In Figure 2-1 the element mesh of the canister can be seen.

2.1.1 Boundary conditions, loading and material

Boundary conditions are defined as symmetry at the symmetry plane. Loads are applied as displacement history at the outer boundary of the copper canister. These displacements are obtained from /Hernelind 2010/. The loading history corresponds to the shear of the BWR canister including the bentonite clay. Three different load steps are applied corresponding to 0, 5 and 10 cm of shear (in the first step there exist initial stresses corresponding to the swelling pressure in the bentonite /Hernelind 2010/). Boundary conditions and loads are shown in Figure 2-2.

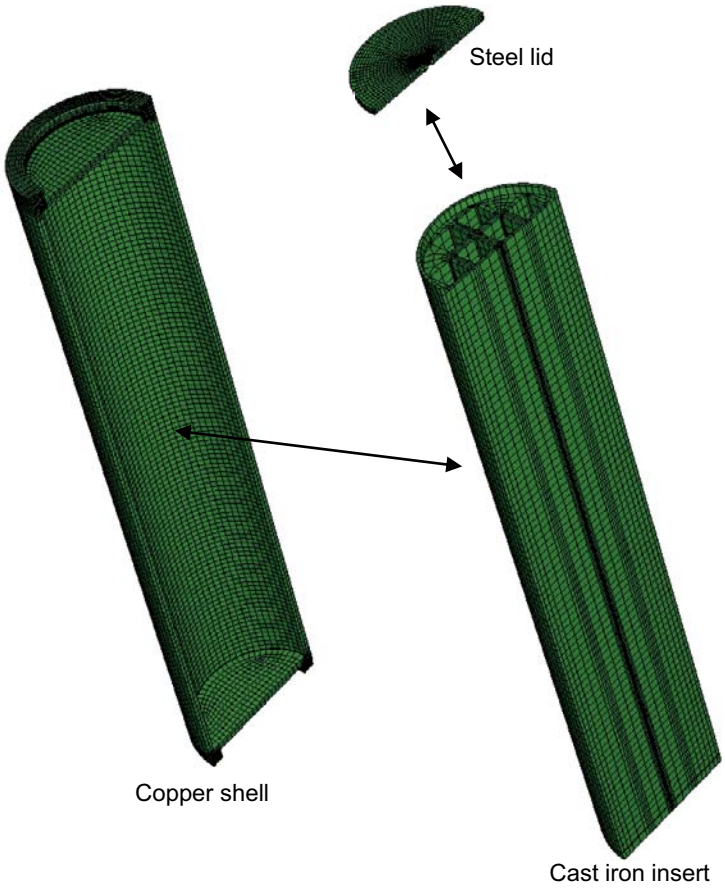

Figure 2-1. *Global model of the BWR canister.*

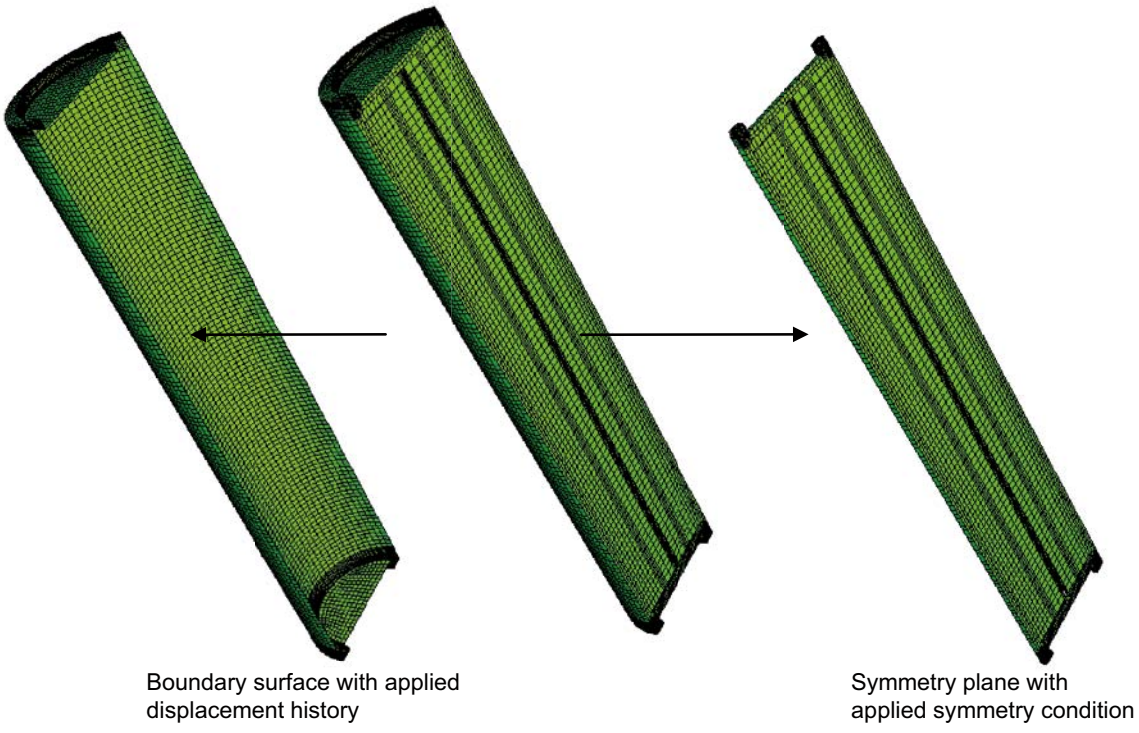

Figure 2-2. *Applied boundary condition and displacement loading.*

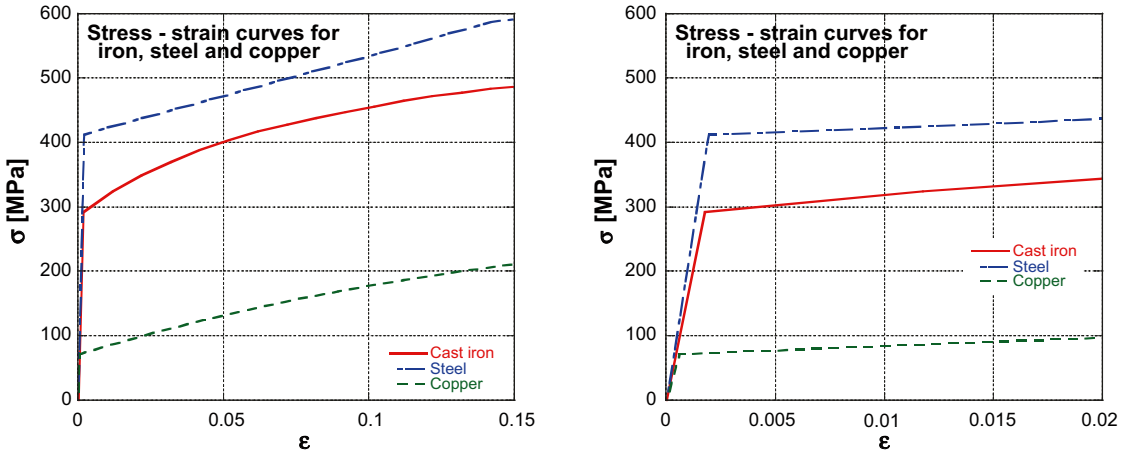

Figure 2-3. True stress – strain curves for copper, steel and cast iron (given at lower strain rates up to $2 \cdot 10^{-4}$ s^{-1}) used in the analyses /Sandström and Andersson 2008, Jin and Sandström 2008, Sandström et al. 2009, SKBdoc 1195044, 1173031, 1201865/.

The materials are defined as elastic-plastic with isotropic hardening. The copper used for the copper shell is modelled with $E = 120$ GPa, $\nu = 0.308$ and $\sigma_y = 72$ Mpa /Sandström and Andersson 2008, Jin and Sandström 2008, Sandström et al. 2009/. The cast iron making up the iron insert is modelled with $E = 166$ GPa, $\nu = 0.32$ and σ_y has a strain rate dependency /SKBdoc 1195044, 1173031, 1201865/. The steel making up the channel tubes is modelled with $E = 210$ GPa, $\nu = 0.30$ and $\sigma_y = 411$ MPa. Stress-strain curves /Sandström and Andersson 2008, Jin and Sandström 2008, Sandström et al. 2009, SKBdoc 1195044, 1173031, 1201865/ are given in Figure 2-3 (using tension tests at lower strain rates up to $2 \cdot 10^{-4}$ s^{-1}). More information on the material models is given in /Hernelind 2010/. Large displacement formulation is used in all analyses.

2.1.2 Results for the global models

The results obtained from the global models in this report are compared with the results obtained by /Hernelind 2010/. The comparison in Table 2-1, 2-2 and 2-3 shows quite small differences. However, the differences can be explained by that the results are dependent on the loading history. The time increment with which the displacement history is applied is not that refined that it gives exactly the same results as those obtained by /Hernelind 2010/. The differences are considered to be small and not to influence the results significantly.

Table 2-1. Comparison for model6g_normal_quarter_1950ca3.

Comparison between Hernelind and Inspectas global model without bentonite clay	Iron insert Max principal stress [MPa]	
	5 cm	10 cm
Hernelind	429.7	456.6
Inspecta	430.0	458.1
Difference [%]	0.0	0.3

Table 2-2. Comparison for model6g_normal_quarter_2000ca3.

Comparison between Hernelind and Inspectas global model without bentonite clay	Iron insert Max principal stress [MPa]	
	5 cm	10 cm
Hernelind	447.0	463.5
Inspecta	447.1	466.9
Difference [%]	0.0	0.7

Table 2-3. Comparison for model6g_normal_quarter_2050ca3.

Comparison between Hernelind and Inspectas global model without bentonite clay		
	Iron insert Max principal stress [MPa] 5 cm	10 cm
Hernelind	455.3	469.7
Inspecta	457.2	472.6
Difference [%]	0.4	0.6

For each global model the results are investigated to decide where to introduce the defect in that model. The location where the max principal stress is the highest is identified, see Figure 2-4. In all the three global models the location identified is roughly the same. In the identified location the submodels containing the defects are introduced (see Section 2.2).

2.2 Submodels at the location with max principal stress

Four different defects are modelled, each with three different crack depths. This gives a total of 12 submodels. All submodels are made up by 20 node brick elements with reduced integration (C3D20R). To check this choice, a comparison was made using the elements C3D20, C3D20R (using reduced integration) and C3D20H (using a hybrid displacement/pressure formulation interpolation scheme). The difference, when comparing the calculated *J*-values, is quite small. In some cases the C3D20R elements introduced problems at the crack tip front. In these cases the C3D20 elements were used instead. All submodels use the same material models as their respective global model, see Figure 2-3. Below the modelling of the four different defects is described. Large displacement formulation is used in all analyses.

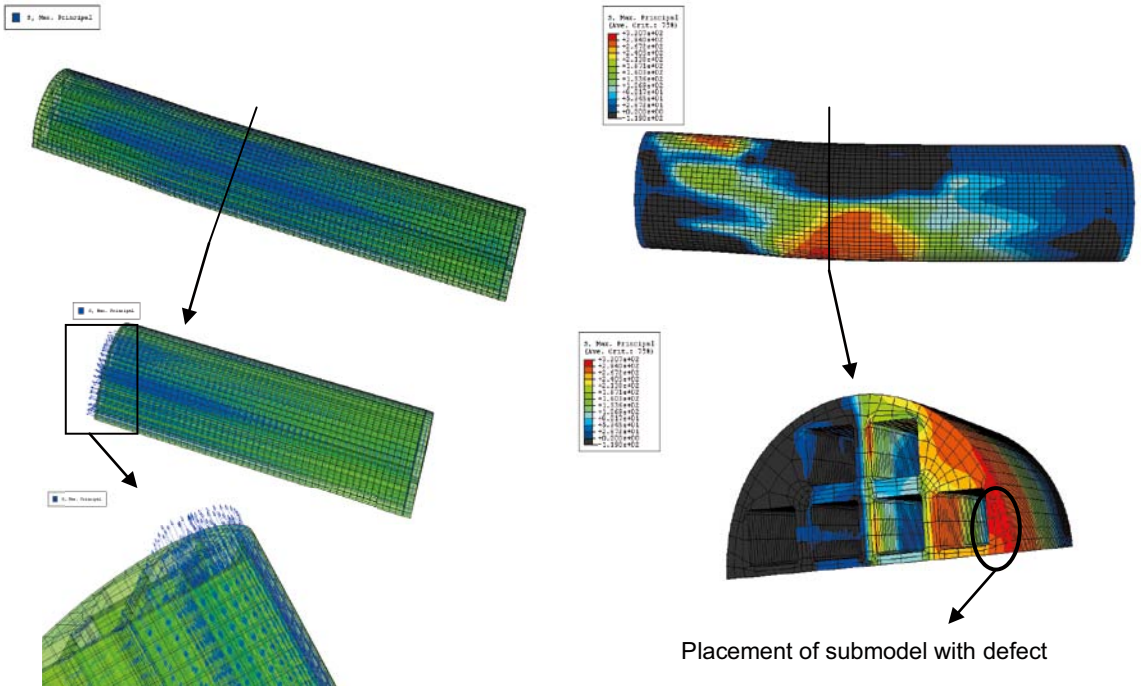

Figure 2-4. *Identified location for submodels containing the defects.*

2.2.1 FE-models of surface defects

Since the submodels containing surface defects are placed at the outer boundary of the cast iron insert, part of the copper canister is also modelled for the submodel. This is done not to neglect any influence from the contact between the copper and iron surfaces. All six submodels are created as two rectangular blocks, one for the copper canister and one for the cast iron casing. The submodels are created with the same external size, independent of defect and crack depth. The geometry of the models are shown in Figure 2-5 with H = 100 mm, w = 120 mm, t_{copper} = 20 mm, t_{iron} = 30 mm, a = 1, 5, 10 mm, for semi-elliptical defect $2c = 6a$ and for semi-circular defect $a = c$. One extra model without a defect is also created to check the accuracy of the submodelling technique. The models are also curved to match the radius of the canister.

The element mesh is focused towards the crack tip. The crack tip is modelled with a small notch as can be seen in Figure 2-6.

To decide the mesh refinement of the crack tip area, a quarter model of the surface crack is created. For the quarter model the variables R_1, R_2, η, μ and MR are held constant while MF and the number of elements along the crack front, NA, are varied (variable definition, see Figure 2-6). From these analyses the J-integral is computed and compared.

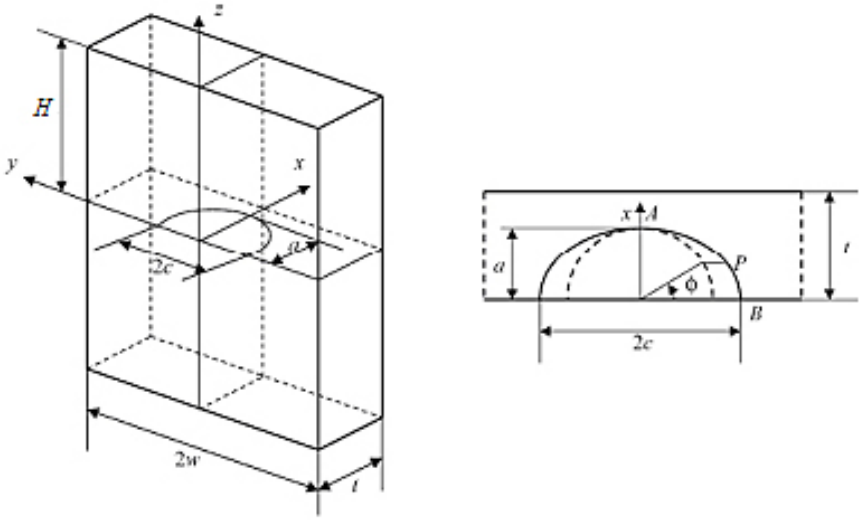

Figure 2-5. *Geometry of a semi-elliptical surface defect.*

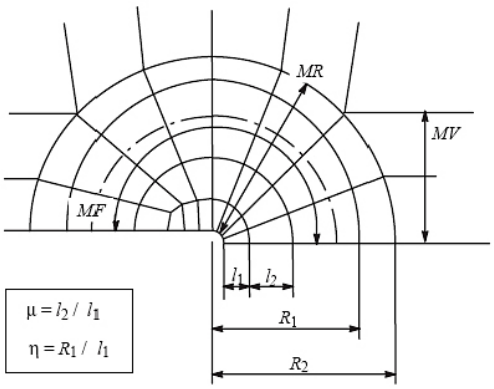

Figure 2-6. *Focused element mesh towards the crack tip.*

In Figure 2-7 the results of these sensitivity analyses are shown. From the sensitivity analyses a crack tip mesh with *MF* = 6, *MR* = 10 *MV* = 2 and 20 elements along the crack front is used in the analysis (since a sufficient number of elements along the crack front is needed).

Below, in Figure 2-8, a typical element mesh of the submodel containing a surface defect is shown.

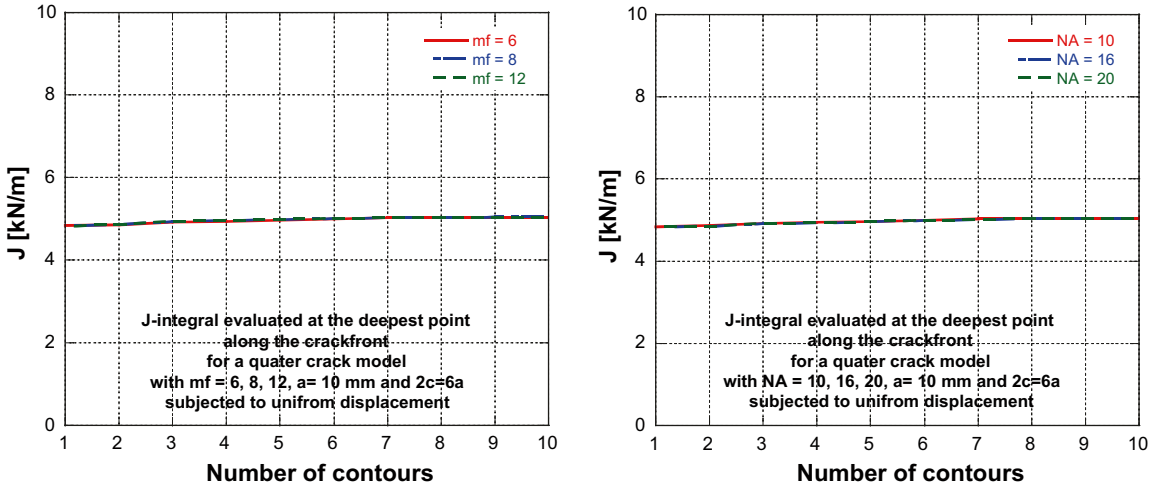

Figure 2-7. *Results from the sensitivity analyses.*

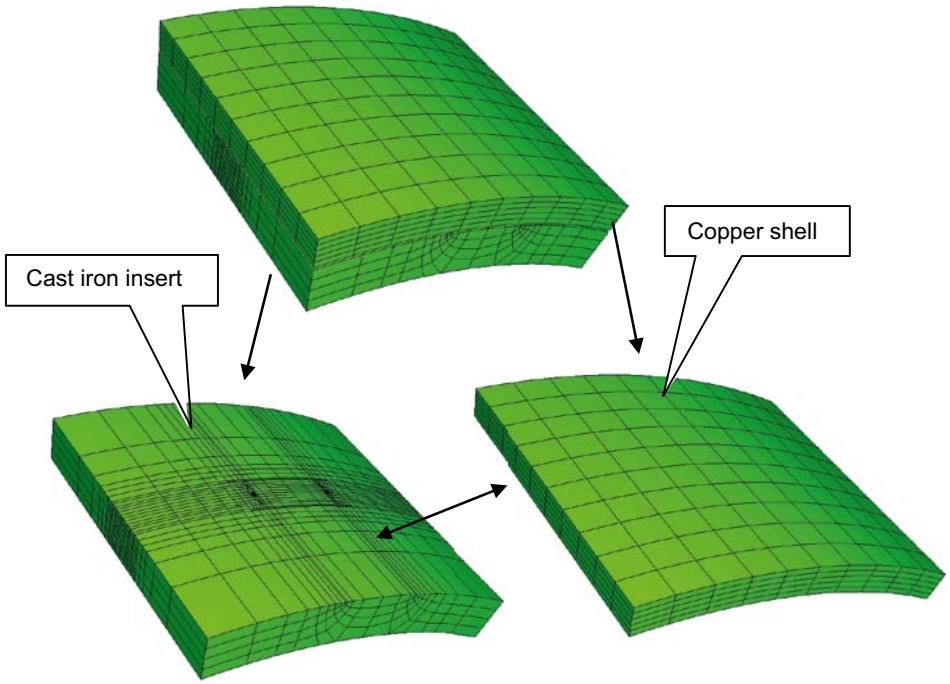

Figure 2-8. *Element mesh for a submodel with a = 10 mm.*

Boundary conditions and loading for the submodel consist of displacements on the boundary obtained from the global model. These are automatically extrapolated from the global model to the boundary of the submodel and hence it is very important that the placement of the submodel relative the global model is correct. In Figure 2-9 the placement of a typical submodel relative the global model is shown.

To check the correctness of the transferred displacements from the global model to the submodel a model without a crack is used. The stresses through the thickness are compared with the corresponding stresses in the global model. The results showed good agreement between the global model and submodel as is shown in Figure 2-10.

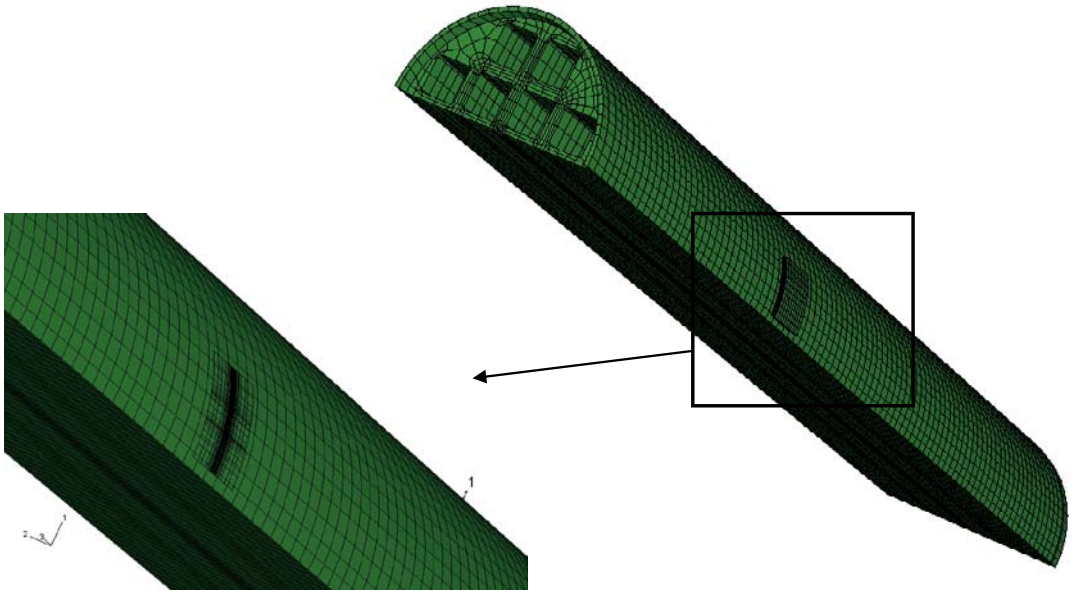

Figure 2-9. *Placement of a submodel relative the global model.*

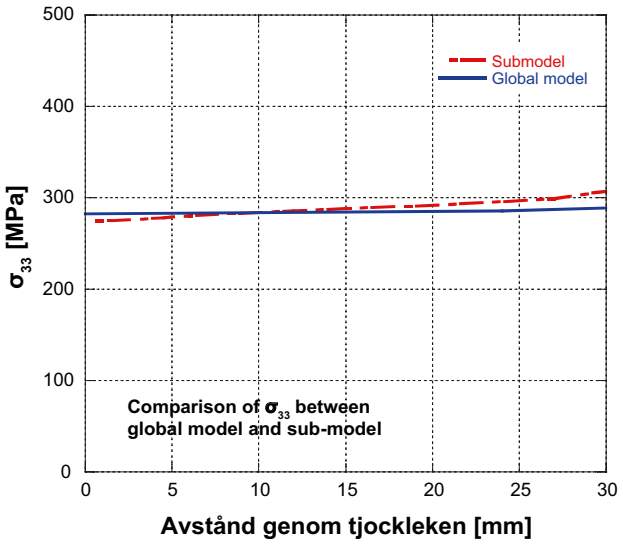

Figure 2-10. *Stresses through the thickness for the submodel and the global model.*

2.2.2 FE-models of internal defects

The submodels containing the elliptical and circular internal defects are created as rectangular blocks containing the defect. Since the submodels containing internal defects are placed at the boundary of the cast iron inserts channel tubes, part of the steel tubes is also modelled for the submodel. The maximum size of the submodel is limited by the smallest thickness between the outer boundary and the channels in the cast iron insert. The chosen sizes used for the different defects were based on a size sensitivity analysis. The geometry for the submodel is shown in Figure 2-11. Three different geometries are used for the three different crack depths as listed below. The elliptical defect is modelled with $2c = 12a$ and the circular with $2c = 2a$.

- 2a = 1 mm:
  H = 30 mm, w = 30 mm and t = 30 mm
- 2a = 5 mm:
  H = 45 mm, w = 45 mm and t = 40 mm
- 2a = 10 mm:
  H = 60 mm, w = 60 mm and t = 45 mm

The element mesh is focused towards the crack tip. The crack tip is modelled with a small notch as can be seen in Figure 2-6. The same mesh setup as for the surface defect is used for the internal defects with the exception of number of elements along the crack front. For the internal defects the number of elements along the crack front is doubled to 40. In Figure 2-12 the element mesh for a typical elliptical defect is shown.

Boundary conditions and loading for the submodel consist of displacements on the boundary obtained from the global model. These are automatically interpolated from the global model to the boundary of the submodel.

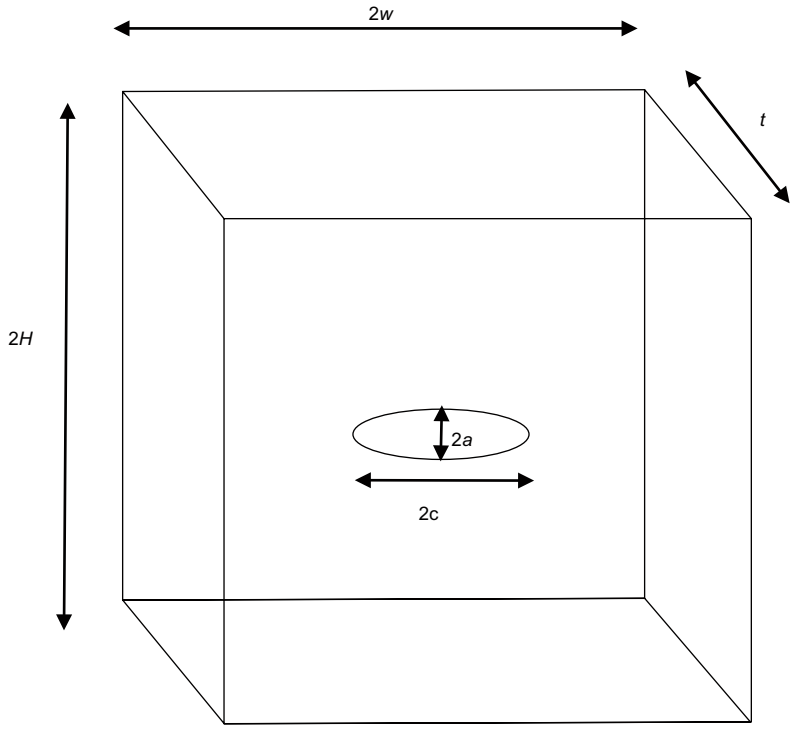

Figure 2-11. *Geometry of the internal defect.*

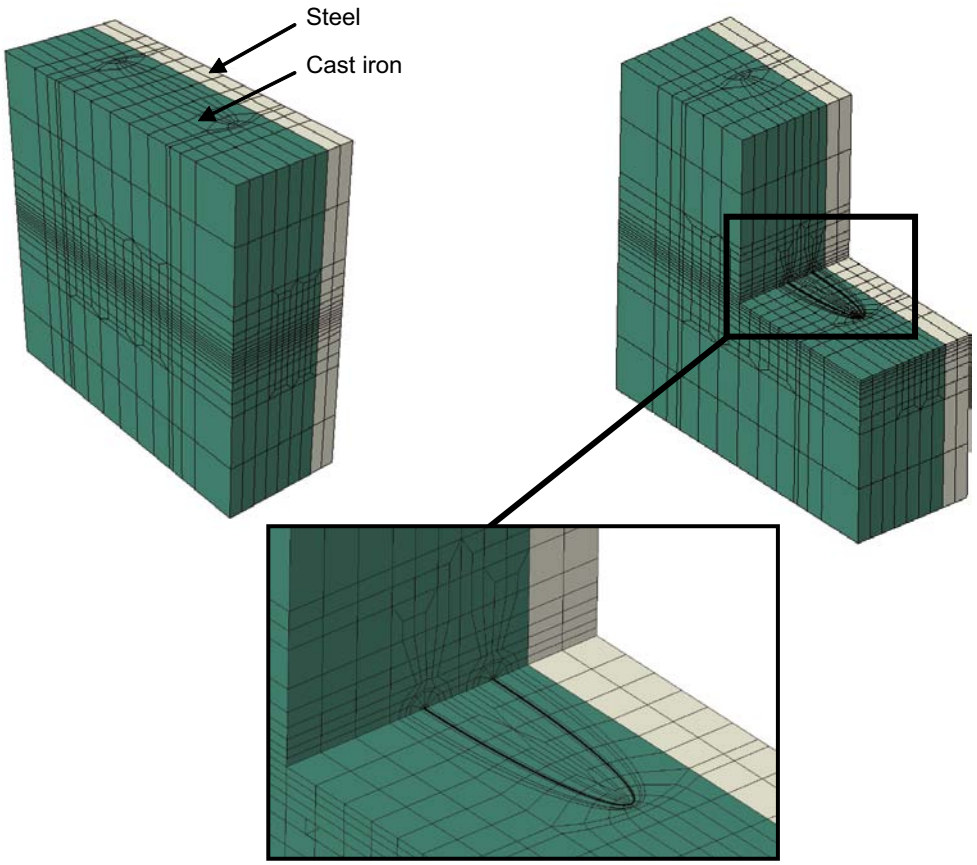

Figure 2-12. *Element mesh for an elliptical internal defect.*

2.2.3 Results at the location with max principal stress component

The results presented below, and in appendix A-C, are obtained using the different submodels. ABAQUS domain integral method is used to calculate the *J*-integral /ABAQUS 2008/. The results are given for *model6g_normal_quarter_1950ca3* in Appendix A, for *model6g_normal_quarter_2000ca3* in Appendix B and for *model6g_normal_quarter_2050ca3* in Appendix C. The results show that the density of the bentonite clay does have an effect on the results. Higher density gives higher *J*-values. It is also seen, as expected, that the elliptical surface defects give much higher *J*-values than the circular surface defects. The internal defects do not give as high *J*-values as the surface defects. These trends between the different types of defects do correspond to handbook solutions for simpler geometries and loading conditions. The maximum *J*-value for the different submodels is summarized in Table 2-4 to 2-7.

Table 2-4. Maximum *J*-value [kN/m], along the crack front, for a semi-elliptical surface defect.

Model	*a* = 1 mm Shear = 5–10 cm		*a* = 5 mm Shear = 5–10 cm		*a* = 10 mm Shear = 5–10 cm	
model6g_normal_quarter_2050ca3	10.42	26.97	49.16	129.00	82.41	219.30
model6g_normal_quarter_2000ca3	5.80	19.16	28.43	94.73	49.45	165.60
model6g_normal_quarter_1950ca3	3.55	10.35	18.15	56.52	31.07	96.85

Table 2-5. Maximum *J*-value [kN/m], along the crack front, for a semi-circular surface defect.

Model	*a* = 1 mm Shear = 5–10 cm		*a* = 5 mm Shear = 5–10 cm		*a* = 10 mm Shear = 5–10 cm	
model6g_normal_quarter_2050ca3	5.93	14.98	28.81	73.74	52.37	136.10
model6g_normal_quarter_2000ca3	3.28	10.67	16.46	54.06	30.80	103.40
model6g_normal_quarter_1950ca3	2.11	6.40	10.60	32.37	19.72	61.31

Table 2-6. Maximum *J*-value [kN/m], along the crack front, for an internal elliptical defect.

Model	2*a* = 1 mm Shear = 5–10 cm		2*a* = 5 mm Shear = 5–10 cm		2*a* = 10 mm Shear = 5–10 cm	
model6g_normal_quarter_2050ca3	3.29	7.13	21.86	56.49	42.95	114.20
model6g_normal_quarter_2000ca3	2.30	6.35	15.71	49.39	34.08	107.20
model6g_normal_quarter_1950ca3	1.95	5.46	10.61	30.27	22.58	64.52

Table 2-7. Maximum *J*-value [kN/m], along the crack front, for an internal circular defect.

Model	2*a* = 1 mm Shear = 5–10 cm		2*a* = 5 mm Shear = 5–10 cm		2*a* = 10 mm Shear = 5–10 cm	
model6g_normal_quarter_2050ca3	1.97	4.71	9.88	25.71	18.43	49.64
model6g_normal_quarter_2000ca3	1.36	4.47	7.06	22.85	13.80	44.66
model6g_normal_quarter_1950ca3	0.90	2.69	4.57	13.67	9.05	26.69

3 Assumptions in the damage tolerance analysis

According to SKB, postulated defects in the location with the highest principal stresses (in tension) should be analyzed.

3.1 Insert geometry and postulated defects

The BWR insert geometry is obtained from the global FE-model by /Hernelind 2010/. For each global model (three models = Model6g_normal_quarter_1950ca3, Model6g_normal_quarter_2000ca3 and Model6g_normal_quarter_2050ca3) the results are investigated to decide where to introduce the defect in that model. The location where the max principal stress component is the highest is identified (see Section 2). In all the three global models the location identified is roughly the same. In the identified location the submodels containing the defects are introduced.

In the damage tolerance analysis, the defects are assumed to be crack like defects even though this type of defects has not been found in the inserts /SKBdoc 1175208/. This is a conservative assumption in the analysis. Four types of defects have been postulated to exist in the insert and are included in the damage tolerance analysis. The geometry of these defects is summarized in Table 3-1.

3.2 Material properties – fracture toughness

In the damage tolerance analysis, defects are postulated in the insert. Therefore, the fracture toughness for the cast iron is needed to do an assessment (at the temperature 0°C, which is relevant for a shear load). It is observed from fracture toughness experiments by the department of solid mechanics (KTH) /SKBdoc 1203550/ that the crack propagation in this material experiences *J*-dominant stable crack growth (see Figure 3-1). Therefore, the fracture toughness data presented in Table 3-2 has data both for initiation and including 2 mm of stable crack growth /SKBdoc 1203550/. Only qualified data, according to ASTM E1820 (Standard Test Method for Measurement of Fracture Toughness), are given in Table 3-2.

Table 3-1. Postulated defects included in the damage tolerance analysis.

Type of defect	Defect depth	Defect length
Semi-elliptical surface crack	a = 1, 5, 10 mm	$2c = 6a$ = 6, 30, 60 mm
Semi-circular surface crack	a = 1, 5, 10 mm	$2c = 2a$ = 2, 10, 20 mm
Elliptical internal crack	$2a$ = 1, 5, 10 mm	$2c = 12a$ = 6, 30, 60 mm
Circular internal crack	$2a$ = 1, 5, 10 mm	$2c = 2a$ = 1, 5, 10 mm

Table 3-2. Fracture toughness data, at 0°C, for the cast iron used in the insert /SKBdoc 1203550/.

Fracture toughness	Data
J_{Ic} [kN/m] At initiation	29, 43, 33, 30, 33, 37, 32, 34, 33, 33 40, 32, 37, 32, 35, 29, 38, 39, 30, 32 39, 43, 37, 30, 31
J_{2mm} [kN/m] At 2 mm stable crack growth	92, 83, 97, 82, 92, 85, 93, 87, 91, 92 99, 72, 97, 81, 77, 97, 101, 108, 92, 90 90, 89, 98, 94, 92

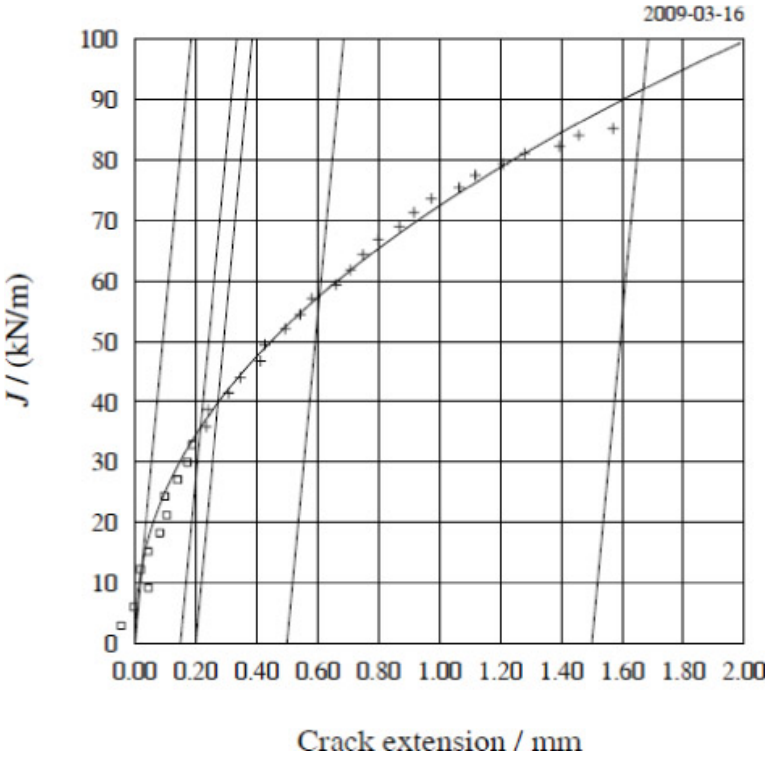

Figure 3-1. *Typical JR-curve from /SKBdoc 1203550/.*

Using the fracture toughness data given in Table 3-2, we can calculate the sample mean value and the sample standard deviation using the equations below. The sample mean value is given as (n = number of samples):

$$m = \frac{1}{n}\sum_{i=1}^{n} x_i \tag{3-1}$$

The unbiased sample standard deviation (the square root of the unbiased sample variance) is given as:

$$s = \sqrt{\frac{1}{n-1}\left[\sum_{i=1}^{n} x_i^2 - \frac{1}{n}\left(\sum_{i=1}^{n} x_i\right)^2\right]} \tag{3-2}$$

From a sample we now have obtained single-valued estimates of the mean and standard deviation of the fracture toughness. These single-valued estimates represent our best estimate of the population values. In a damage tolerance analysis we want to use an estimate with a given confidence (i.e. 90%). Thus we are interested in the accuracy of these sample estimates. Confidence intervals represent a means of providing a range of values in which the true value can be expected to lie. In this investigation we will use approximate confidence intervals, using properties of the so-called Student's t-distribution and the χ^2-distribution /Ayyub and McCuen 1997/.

Confidence interval for the population mean μ, when the population standard deviation σ is unknown, has the following form:

$$m - t_{\alpha/2,n-1}\left(\frac{s}{\sqrt{n}}\right) \le \mu \le m + t_{\alpha/2,n-1}\left(\frac{s}{\sqrt{n}}\right) \tag{3-3}$$

where $t_{\alpha/2,\,n-1}$ is the Student's t-distribution (using a two-sided interval) with a level of significance α and with n–1 degrees of freedom.

The confidence intervals given above now provide an interval in which we are 100(1–α) percent confident that the population values lies within that given interval. Using the data from /SKBdoc 1203550/ we now can calculate estimates and confidence intervals for different fracture toughness distributions (J_{Ic} or J_{2mm}). These calculations are summarized in Table 3-3.

Table 3-3. Evaluated fracture toughness data. Estimates of the population mean (using α = 0.1, i.e. 90% confidence).

Case	Sample mean m	Population mean μ
J_{Ic} [kN/m]	34.4	$33.0 \leq \mu \leq 35.9$
J_{2mm} [kN/m]	90.8	$88.1 \leq \mu \leq 93.5$

Conservative fracture toughness data, to be used in a damage tolerance analysis (with 90% confidence), is therefore $J_{Ic} = 33$ kN/m or $J_{2mm} = 88$ kN/m.

In this study, stress-strain data at higher strain rates are used /Hernelind 2010/. This means that one has to check if the fracture toughness data given above can be used also at higher strain rates. Such fracture toughness experiments have recently been conducted by the department of solid mechanics (KTH) /SKBdoc 1226428/ and the conclusion is that the data given above can also be used at higher strain rates /SKBdoc 1226428/.

3.3 Failure criteria and safety margins

In the damage tolerance analysis, with postulated defects, the critical defect size is given using the failure criteria $J = J_{mat}$ and the acceptable defect size is given using the criteria $J = J_{mat}/SF_J$. In these equations, J is the applied J-value as given in Section 2.3, J_{mat} is the fracture toughness (with or without some stable crack growth) of the cast iron used in the insert. SF_J is the safety factor used when calculating the acceptable defect size.

As shown in Section 3.2, the cast iron has predominantly ductile fracture behaviour. This means that the material does not break when J reaches the initiation toughness ($J_{mat} = J_{Ic}$), instead the material experiences stable crack growth. According to a recently published investigation from the Swedish Radiation Safety Authority (SSM) /Brickstad 2009/, it is reasonable to use a toughness value at 2 mm of stable crack growth for a ductile material. This is especially true in this case, since the insert is subjected to a short-term displacement controlled loading (i.e. not in load control and therefore could be considered as a secondary load) and there has not been found any crack-like defects in the inserts /SKBdoc 1175208/. Therefore, J_{mat} should be equal to J_{2mm} in this case.

For the choice of safety factor SF_J, the objective has been to retain the safety margins expressed in ASME Sect. XI /ASME 2008/. This means that $SF_J = 10$ is used in the case of normal operation or with loads that occur quite frequently. $SF_J = 2$ is then used for loads with a very low probability of occurrence. According to the design premises for the canister /SKB 2009/, the probability of occurrence is approximately 6.7E-4 (in the case of a 5 cm shear movement during an earthquake). Therefore, SF_J should be equal to 2 in this case.

4 Damage tolerance analysis at the location with max principal stress

In this section, the results from the damage tolerance analysis (at the location with max principal stress) are given. In the analysis the following assumptions have been made:

- The fracture toughness value used is $J_{2mm} = 88$ kN/m (given at 0°C).
- Maximum J-value, along the crack front is used in the analysis (see Table 2-4–2-7).
- When calculating critical defect sizes, the safety factor $SF_J = 1.0$.
- When calculating acceptable defect sizes, the safety factor $SF_J = 2.0$.

4.1 Accepted defect size for internal defects

Table 4-1. Acceptable and critical defect sizes for postulated internal elliptical defects.

Model	Acceptable depth Shear = 5–10 cm		Acceptable length Shear = 5–10 cm	
model6g_normal_quarter_2050ca3	> 10	4.0	> 60	24.0
model6g_normal_quarter_2000ca3	> 10	4.5	> 60	27.0
model6g_normal_quarter_1950ca3	> 10	7.0	> 60	42.0
Model	**Critical depth Shear = 5–10 cm**		**Critical length Shear = 5–10 cm**	
model6g_normal_quarter_2050ca3	> 10	7.7	> 60	46.2
model6g_normal_quarter_2000ca3	> 10	8.3	> 60	49.8
model6g_normal_quarter_1950ca3	> 10	> 10	> 60	> 60

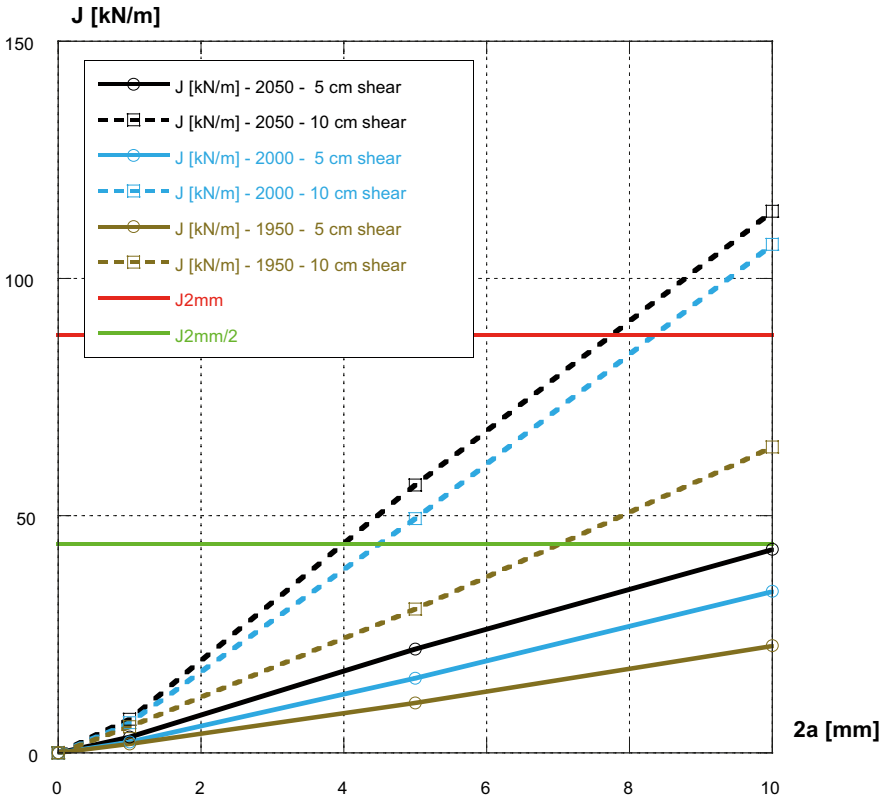

Figure 4-1. *Damage tolerance analysis for postulated internal elliptical defects.*

Table 4-2. Acceptable and critical defect sizes for postulated internal circular defects.

Model	Acceptable depth Shear = 5–10 cm		Acceptable length Shear = 5–10 cm	
model6g_normal_quarter_2050ca3	> 10	8.8	> 10	8.8
model6g_normal_quarter_2000ca3	> 10	9.8	> 10	9.8
model6g_normal_quarter_1950ca3	> 10	> 10	> 10	> 10
Model	**Critical depth Shear = 5–10 cm**		**Critical length Shear = 5–10 cm**	
model6g_normal_quarter_2050ca3	> 10	> 10	> 10	> 10
model6g_normal_quarter_2000ca3	> 10	> 10	> 10	> 10
model6g_normal_quarter_1950ca3	> 10	> 10	> 10	> 10

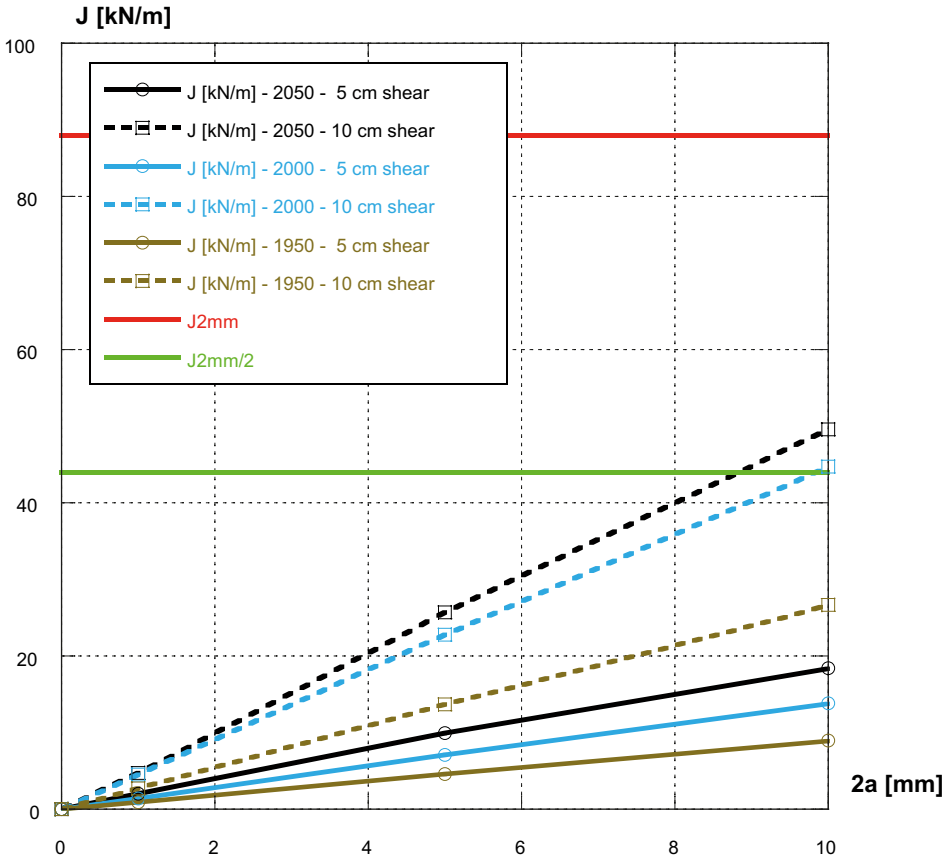

Figure 4-2. *Damage tolerance analysis for postulated internal circular defects.*

4.2 Accepted defect size for surface defects

Table 4-3. Acceptable and critical defect sizes for postulated semi-elliptical surface cracks.

Model	Acceptable depth Shear = 5–10 cm		Acceptable length Shear = 5–10 cm	
model6g_normal_quarter_2050ca3	4.5	1.7	27.0	10.2
model6g_normal_quarter_2000ca3	8.7	2.3	52.2	13.8
model6g_normal_quarter_1950ca3	> 10	3.9	> 60	23.4
Model	**Critical depth Shear = 5–10 cm**		**Critical length Shear = 5–10 cm**	
model6g_normal_quarter_2050ca3	> 10	3.4	> 60	20.4
model6g_normal_quarter_2000ca3	> 10	4.7	> 60	28.2
model6g_normal_quarter_1950ca3	> 10	8.9	> 60	53.4

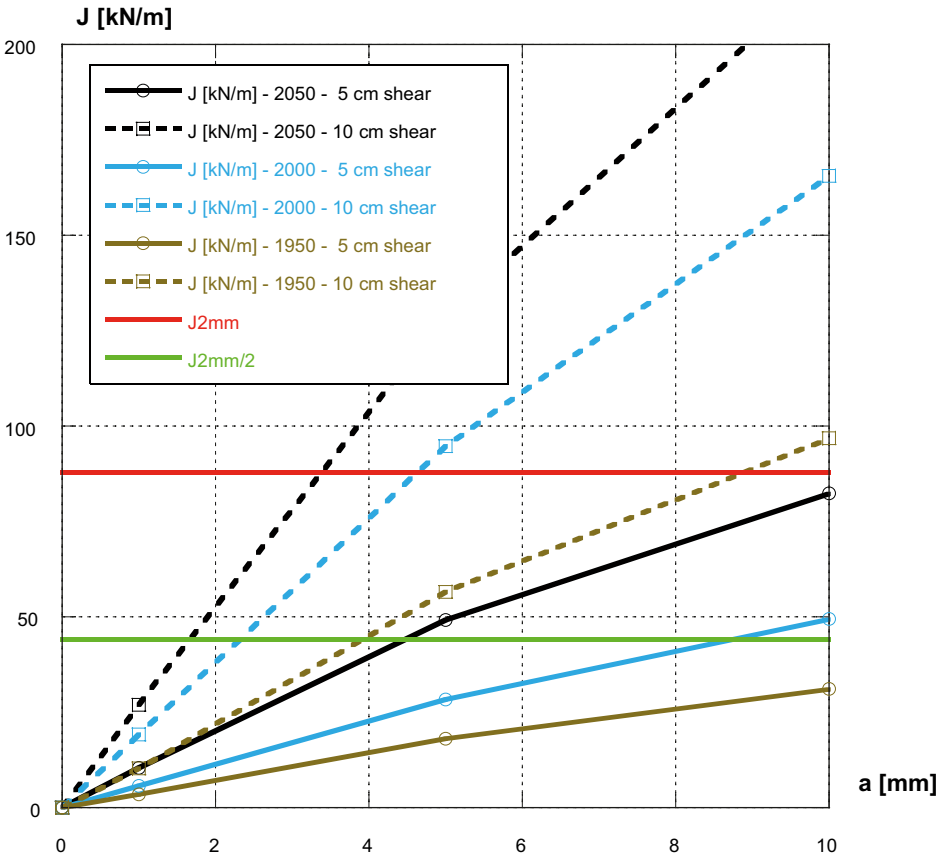

Figure 4-3. *Damage tolerance analysis for postulated semi-elliptical surface cracks.*

Table 4-4. Acceptable and critical defect sizes for postulated semi-circular surface cracks.

Model	Acceptable depth Shear = 5–10 cm		Acceptable length Shear = 5–10 cm	
model6g_normal_quarter_2050ca3	8.2	3.0	16.4	6.0
model6g_normal_quarter_2000ca3	> 10	4.1	> 20	8.2
model6g_normal_quarter_1950ca3	> 10	7.0	> 20	14.0
Model	**Critical depth Shear = 5–10 cm**		**Critical length Shear = 5–10 cm**	
model6g_normal_quarter_2050ca3	> 10	6.2	> 20	12.4
model6g_normal_quarter_2000ca3	> 10	8.4	> 20	16.8
model6g_normal_quarter_1950ca3	> 10	> 10	> 20	> 20

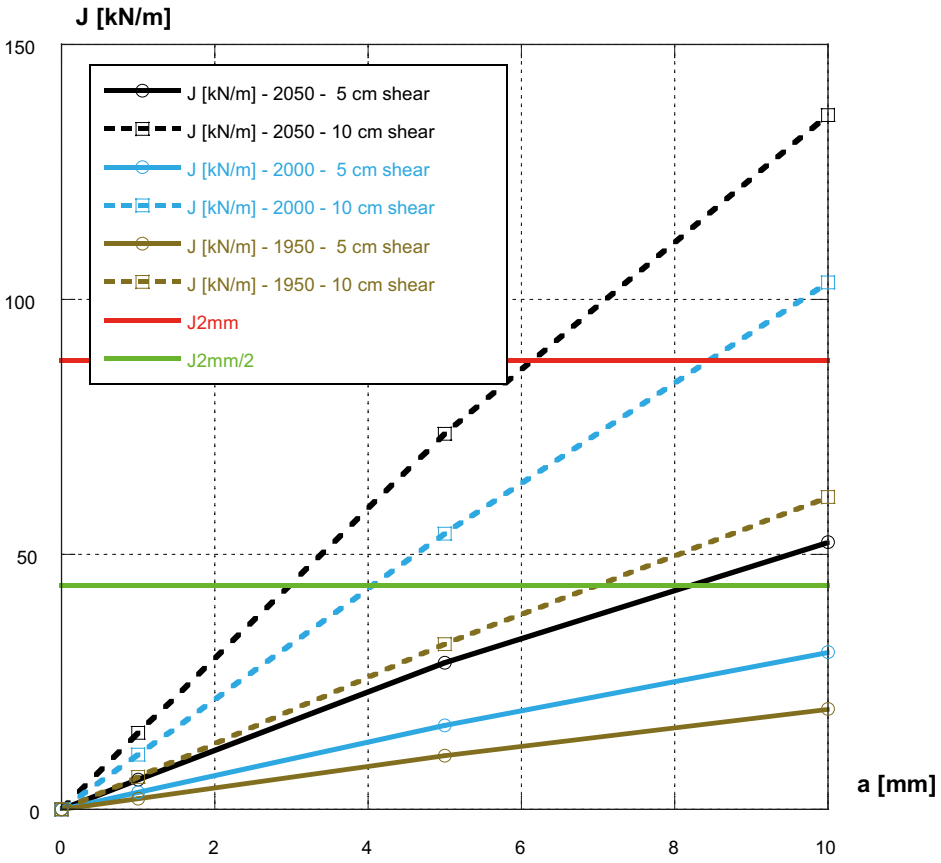

Figure 4-4. *Damage tolerance analysis for postulated semi-circular surface cracks.*

5 Sensitivity study

5.1 Influence of bentonite clay density

The results presented above show that the density of the bentonite clay does have an important effect on the calculations. Higher density gives higher *J*-values and smaller accepted defect sizes. It is also seen, as expected, that the elliptical surface defects give much higher *J*-values than the circular surface defects (for a given defect depth). The internal defects do not give as high *J*-values as the surface defects. Therefore, the most severe postulated defect is an elliptical surface defect as given in Figure 5-1.

When doing non-destructive testing of the inserts, a surface method may be used. In this case it is more interesting to consider the acceptable defect length (see Figure 5-2).

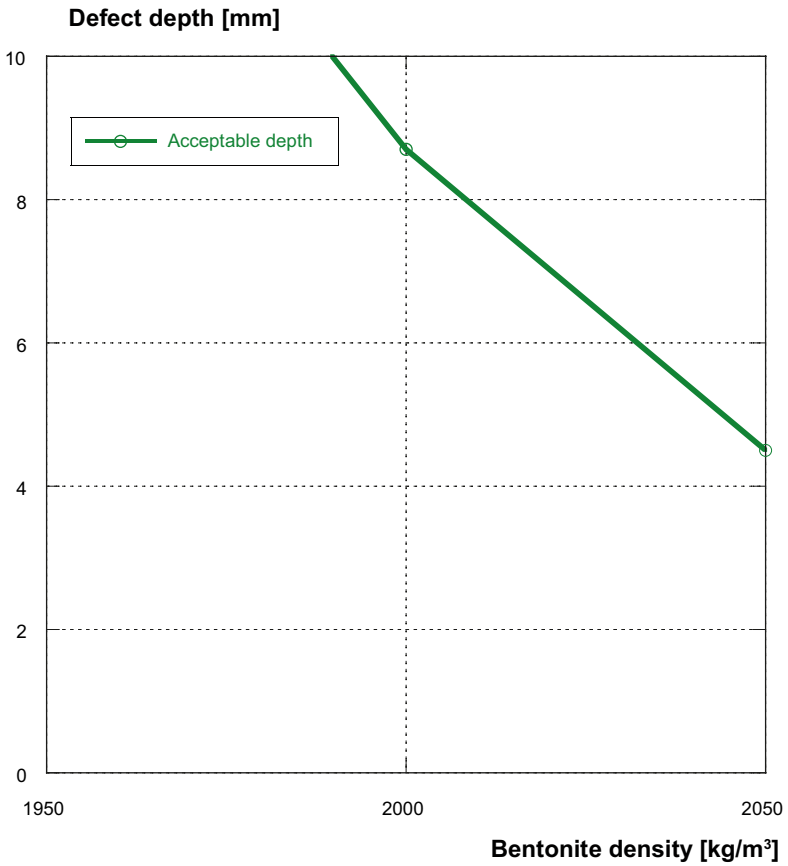

Figure 5-1. *Acceptable defect depth for postulated semi-elliptical surface cracks (shear = 5 cm). The critical defect depth is always larger than 10 mm.*

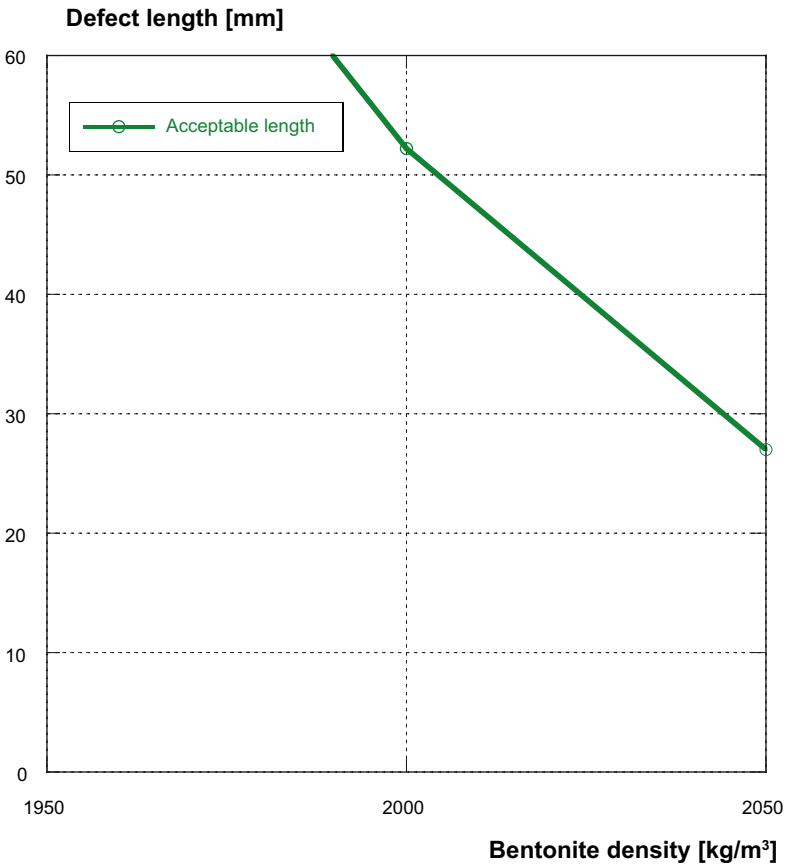

Figure 5-2. *Acceptable defect length for postulated semi-elliptical surface cracks (shear = 5 cm). The critical defect length is always larger than 60 mm.*

5.2 Comparison between different defect geometry assumptions

It is possible to calculate the most probable critical defect depth, using the four different types of defect geometries considered in this study. In this case we use best estimates regarding bentonite density (a uniform distribution) and fracture toughness (a normal distribution using data from Section 3.2) of the insert. The result from such an analysis, using Monte Carlo Simulation with $N = 10^6$ simulations /Dillström et al. 2008/, is presented in Figure 5-3.

The results given in Figure 5-3 are an estimate on how severe different types of defects are to the integrity of the insert. Obviously, internal defects are less important than surface defects. Also, it should be emphasized that all the analysed defects are oriented in the circumferential direction (this is the worst case), acceptable defect sizes for defects oriented in the axial direction are much larger.

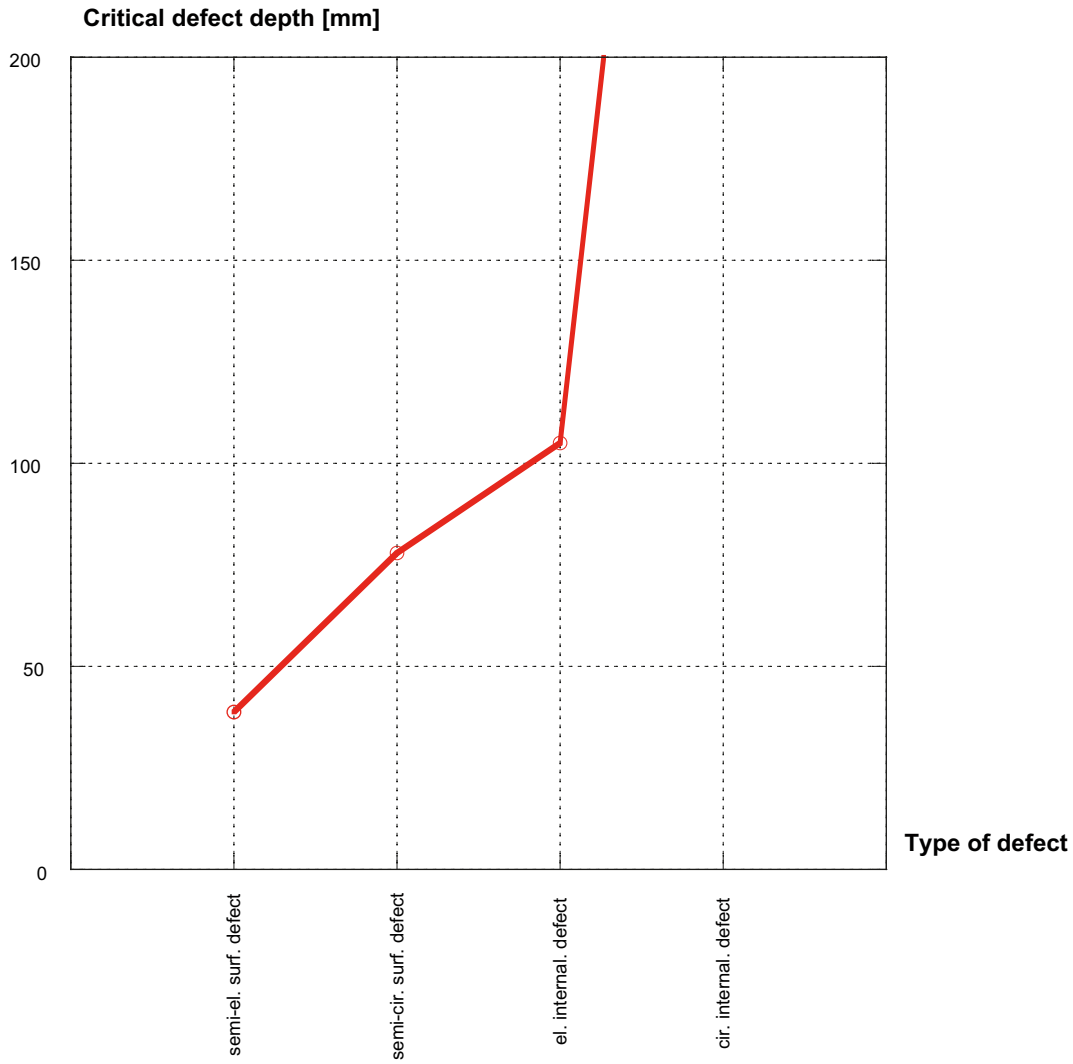

Figure 5-3. *The most probable critical defect depth, using four different kinds of defects.*

6 Summary and conclusions

SKB has asked Inspecta Technology AB to perform a damage tolerance analysis of the cast iron insert for the case of an earthquake induced rock shear load. This report contains results of a fracture mechanics analysis of the insert with postulated defects. The aim of the analyses is to calculate acceptable defect sizes with regard to safety margins against fracture.

Defects are postulated at a location where the max principal stress is the highest (at the outer surface of the insert).

Results from the damage tolerance analysis show that the density of the bentonite clay has an important effect on the calculations. The main conclusions are:

- Higher density gives higher *J*-values and smaller accepted defect sizes.
- It is also seen that the elliptical surface defects give much higher *J*-values than the circular surface defects.
- The internal defects do not give as high *J*-values as the surface defects.
- For the design case, bentonite density = 2,050 kg/m^3 and shear = 5 cm, the acceptable defect depth = 4.5 mm and the acceptable defect length = 27.0 mm (using the most severe defect geometry assumption of a postulated semi-elliptical surface crack). Other defect geometry assumptions, defect locations and defect orientations give larger acceptable defect sizes.

7 References

SKB's (Svensk Kärnbränslehantering AB) publications can be found at www.skb.se/publications. References to SKB's unpublished documents are listed separately at the end of the reference list. Unpublished documents will be submitted upon request to document@skb.se.

ABAQUS, 2008. Abaqus manuals, ver 6.8. Providence, RI: Dassault Systèmes Simulia Corp.

ASME, 2008. ASME boiler and pressure vessel code, section XI. Rules for inservice inspection of nuclear power plant components. New York: American Society of Mechanical Engineers.

Ayyub B M, McCuen R H, 1997. Probability, statistics & reliability for engineers. Boca Raton: CRC Press.

Brickstad B, 2009. Analys av driftinducerade skador i svenska kärntekniska anläggningar. SSM 2008/232, Strålsäkerhetsmyndigheten.

Dillström P, Bergman M, Brickstad B, Zang W, Sattari-Far I, Andersson P, Sund G, Dahlberg L, Nilsson F, 2008. A combined deterministic and probabilistic procedure for safety assessment of components with cracks: handbook. SSM 2008:01, Strålsäkerhetsmyndigheten.

Dillström P, Alverlind L, Andersson M, 2010. Framtagning av acceptanskriterier samt skadetålighetsanalyser av segjärnsinsatsen. SKB R-10-11, Svensk Kärnbränslehantering AB.

Hernelind J, 2010. Modelling and analysis of canister and buffer for earthquake induced rock shear and glaciar load. SKB TR-10-34, Svensk Kärnbränslehantering AB.

Jin L-Z, Sandström R, 2008. Creep of copper canisters in power-law breakdown. Computational Materials Science, 43, pp 403–416.

Sandström R, Andersson H C M, 2008. Creep in phosphorus alloyed copper during power-law breakdown. Journal of Nuclear Materials, 372, pp 76–88.

Sandström R, Hallgren J, Burman G, 2009. Stress strain flow curves for Cu-OFP. SKB R-09-14, Svensk Kärnbränslehantering AB.

SKB, 2009. Design premises for a KBS-3V repository based on results from the safety assessment SR-Can and some subsequent analyses. SKB TR-09-22, Svensk Kärnbränslehantering AB.

Unpublished documents.

SKBdoc id, version	Title	Issuer, year
1173031 ver 1.0	JRC_Compression Experiments adressing Canister Inserts I24 and I25 (NSU/PM/0408.001) Technical Note Note TN.P.04.098.	SKB, 2004
1175208 ver 5.0	Tillverkning av kapselkomponenter.	SKB, 2009
1195044 ver 1.0	JRC_SAFE-CASK Institutional Action Statistical Analysis of Engineering Tensile Properties of Canister Insert Material Interim Report TN.P.04.100.	SKB, 2004
1201865 ver 1.0	Dragprovning av gjutjärn, PM SKB0903c, KTH.	SKB, 2009
1203550 ver 1.0	Brottmekanisk provning gjutjärn, SKB0903, KTH.	SKB, 2009
1226428 ver 1.0	Brottmekanisk provning av gjutjärn SKB91201, KTH.	SKB, 2009

Appendix A

Calculated *J*-values when using a bentonite density of 1,950 kg/m^3

The results below (for the model *model6g_normal_quarter_1950ca3*) are presented in graphs, using one graph for each type of defect and crack depth. In each graph results along the crack front from two different load magnitudes are plotted (the angle ϕ is defined in Figure 2-5). Each load magnitude corresponds to 5 and 10 cm shear of the BWR canister including the bentonite clay.

A1 *J*-values for a semi-elliptical surface defect, using a bentonite density of 1,950 kg/m^3

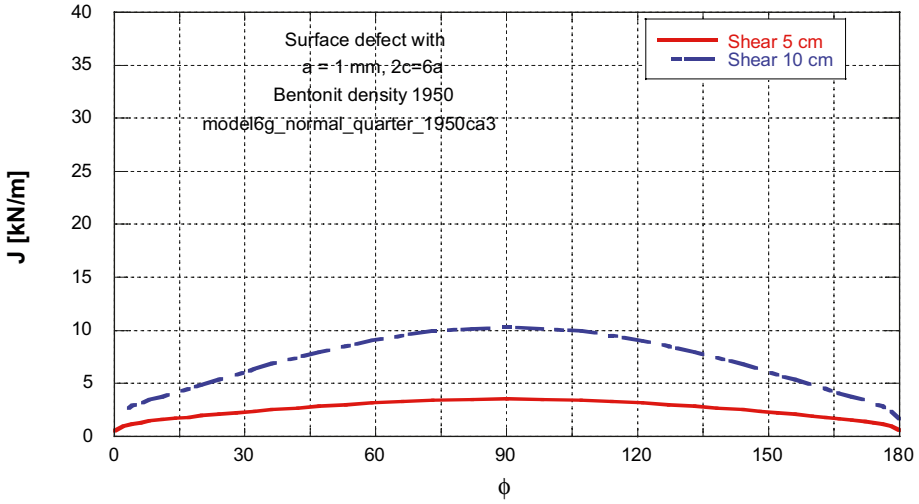

Figure A-1. *J-integral for a semi-elliptical surface defect plotted along the crack front (a = 1 mm).*

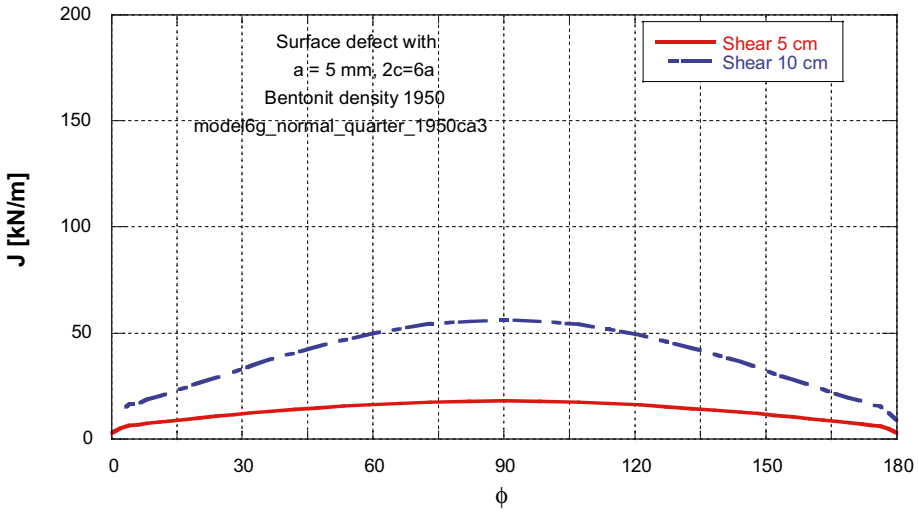

Figure A-2. *J-integral for a semi-elliptical surface defect plotted along the crack front (a = 5 mm).*

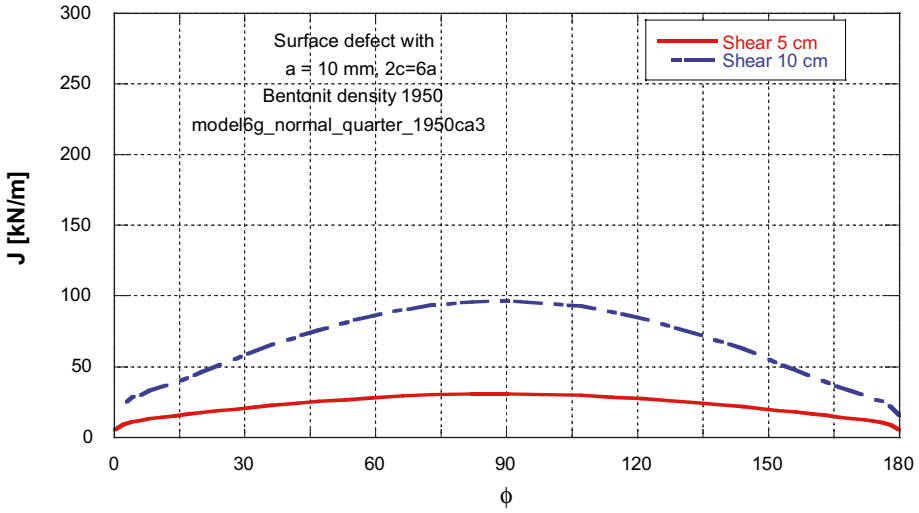

Figure A-3. *J-integral for a semi-elliptical surface defect plotted along the crack front (a = 10 mm).*

A2 *J*-values for a semi-circular surface defect, using a bentonite density of 1,950 kg/m³

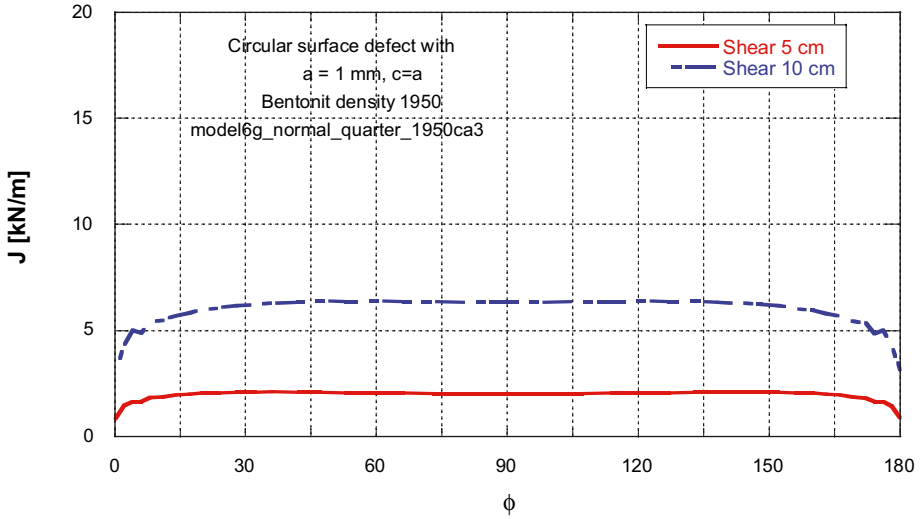

Figure A-4. *J-integral for a semi-circular surface defect plotted along the crack front (a = 1 mm).*

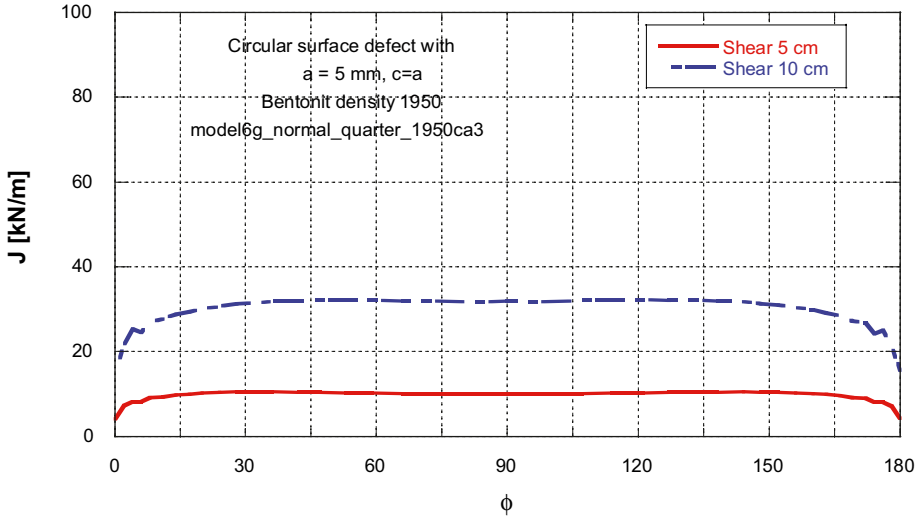

Figure A-5. *J-integral for a semi-circular surface defect plotted along the crack front (a = 5 mm).*

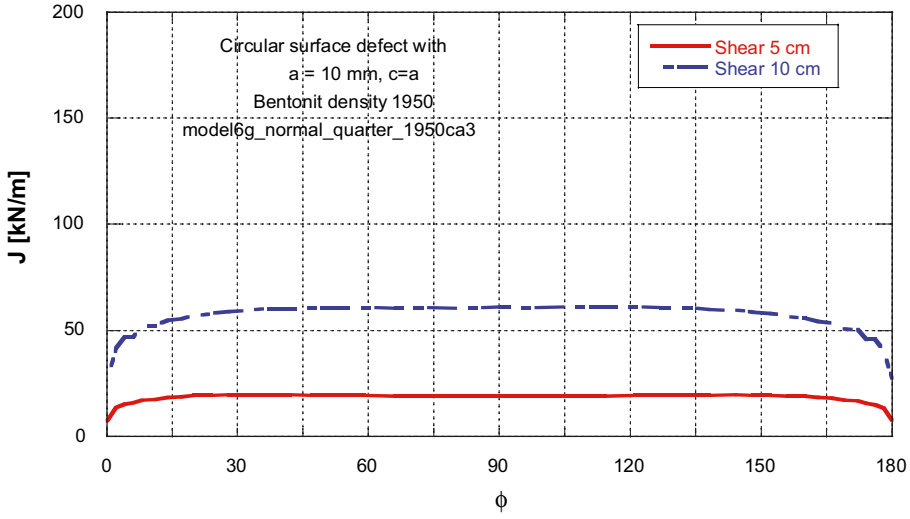

Figure A-6. *J-integral for a semi-circular surface defect plotted along the crack front (a = 10 mm).*

A3 *J*-values for an internal elliptical defect, using a bentonite density of 1,950 kg/m³

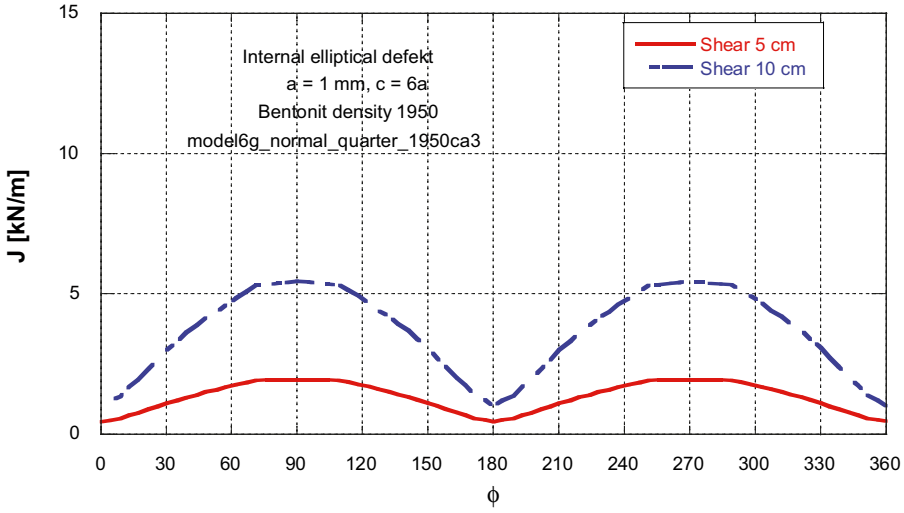

Figure A-7. *J-integral for an internal elliptical defect plotted along the crack front (2a = 1 mm).*

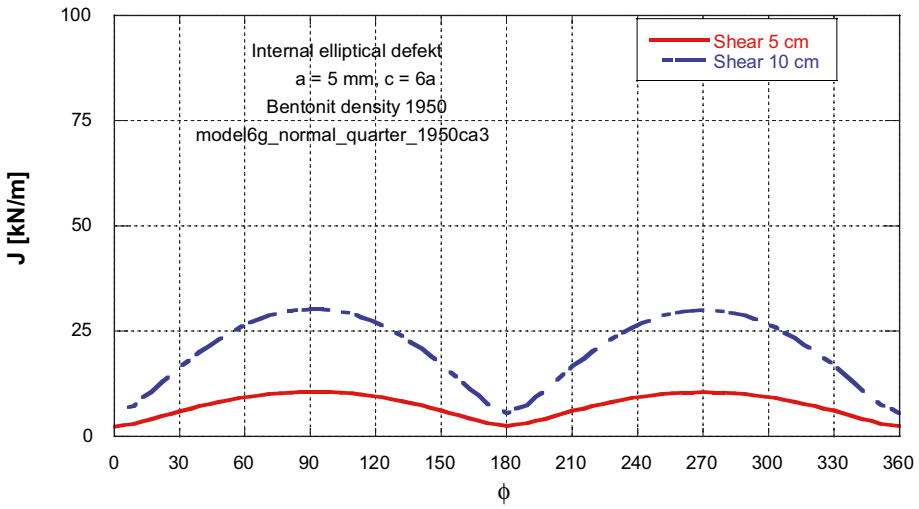

Figure A-8. *J-integral for an internal elliptical defect plotted along the crack front (2a = 5 mm).*

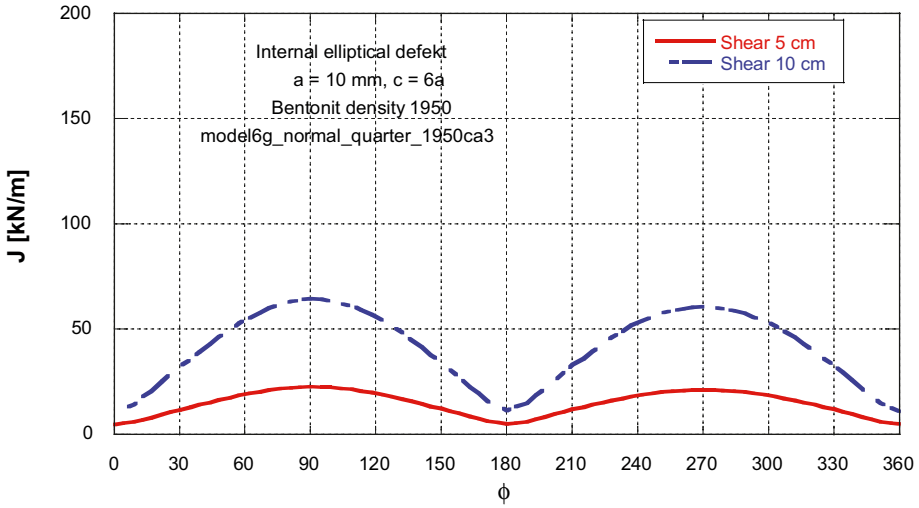

Figure A-9. *J-integral for an internal elliptical defect plotted along the crack front (2a = 10 mm).*

A4 *J*-values for an internal circular defect, using a bentonite density of 1,950 kg/m³

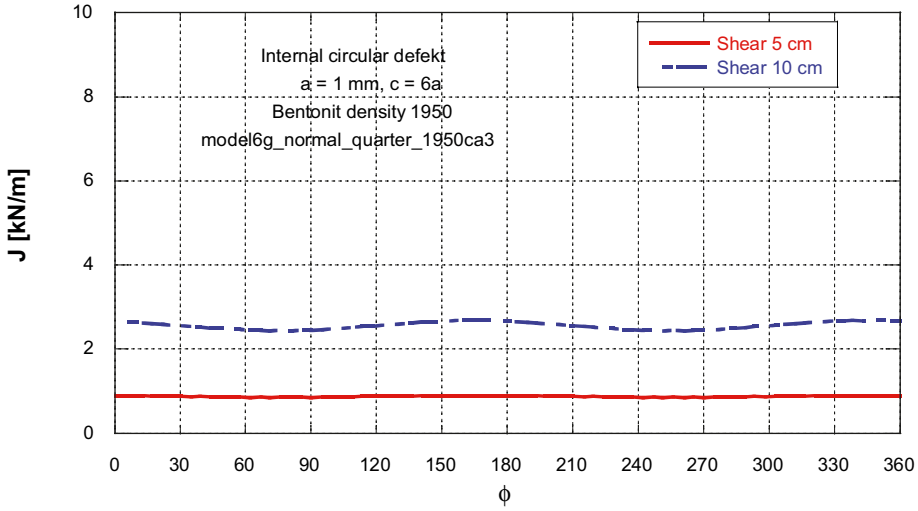

Figure A-10. *J-integral for an internal circular defect plotted along the crack front (2a = 1 mm).*

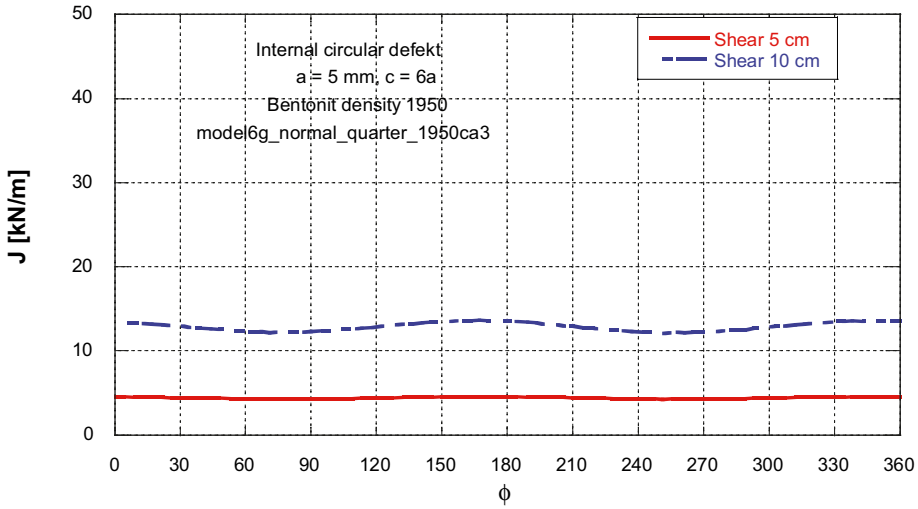

Figure A-11. *J-integral for an internal circular defect plotted along the crack front (2a = 5 mm).*

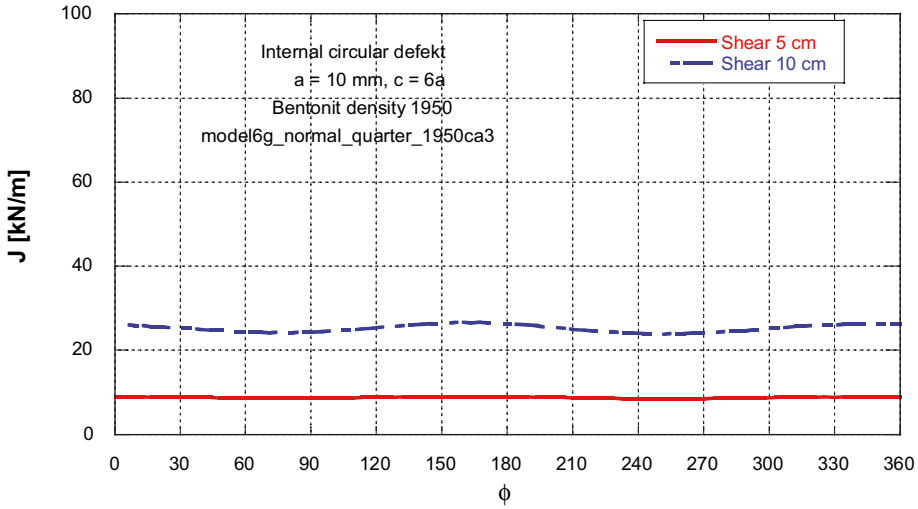

Figure A-12. *J-integral for an internal circular defect plotted along the crack front (2a = 10 mm).*

Appendix B

Calculated *J*-values when using a bentonite density of 2,000 kg/m^3

The results below (for the model *model6g_normal_quarter_2000ca3*) are presented in graphs, using one graph for each type of defect and crack depth. In each graph results along the crack front from two different load magnitudes are plotted (the angle ϕ is defined in Figure 2-5). Each load magnitude corresponds to 5 and 10 cm shear of the BWR canister including the bentonite clay.

B1 *J*-values for a semi-elliptical surface defect, using a bentonite density of 2,000 kg/m^3

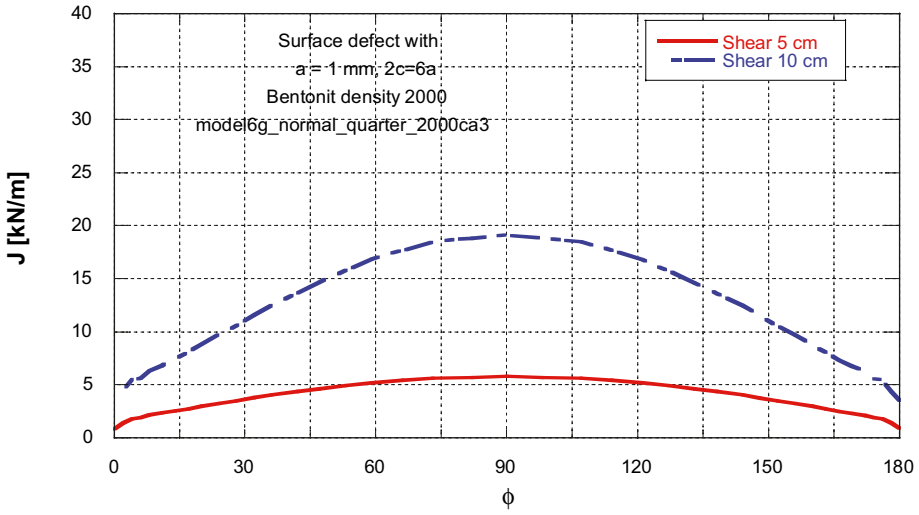

Figure B-1. *J-integral for a semi-elliptical surface defect plotted along the crack front (a = 1 mm).*

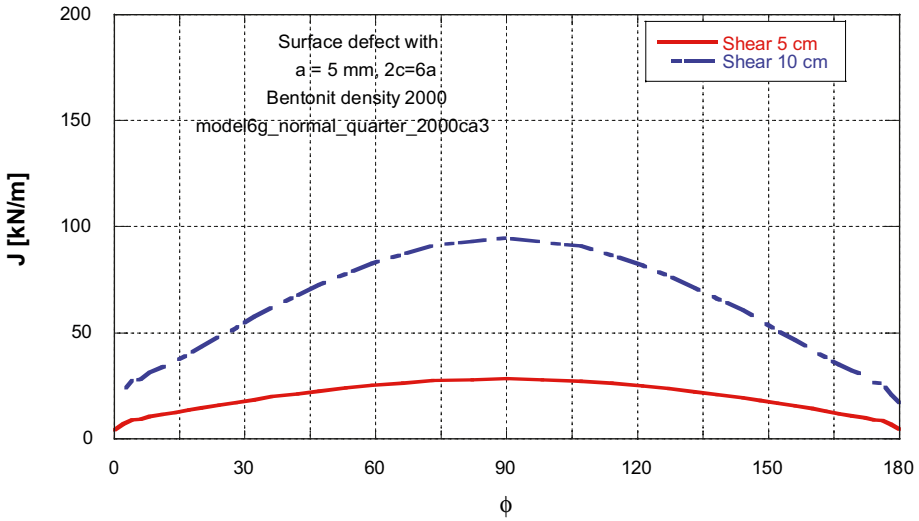

Figure B-2. *J-integral for a semi-elliptical surface defect plotted along the crack front (a = 5 mm).*

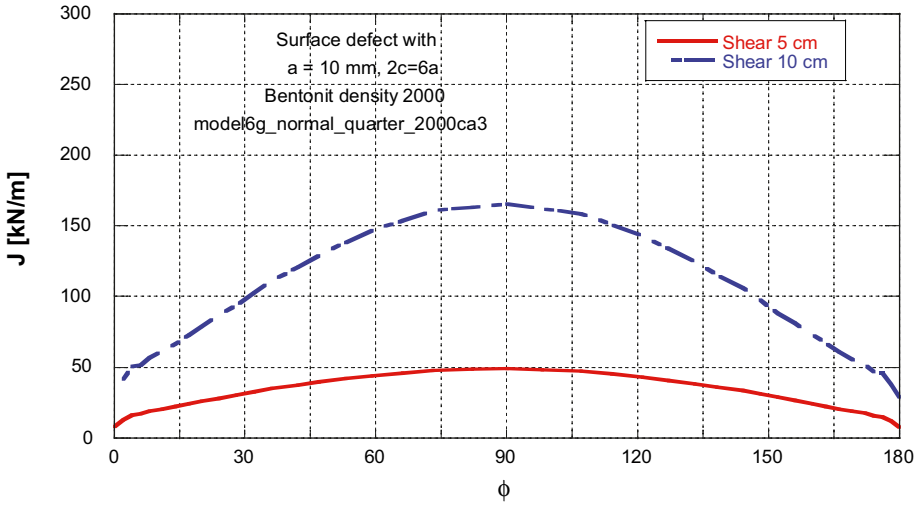

Figure B-3. *J-integral for a semi-elliptical surface defect plotted along the crack front (a = 10 mm).*

B2 *J*-values for a semi-circular surface defect, using a bentonite density of 2,000 kg/m³

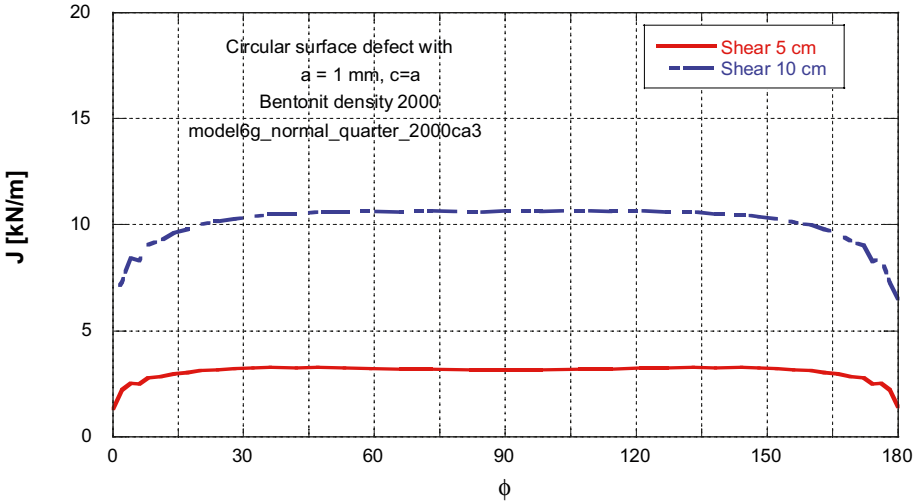

Figure B-4. *J-integral for a semi-circular surface defect plotted along the crack front (a = 1 mm).*

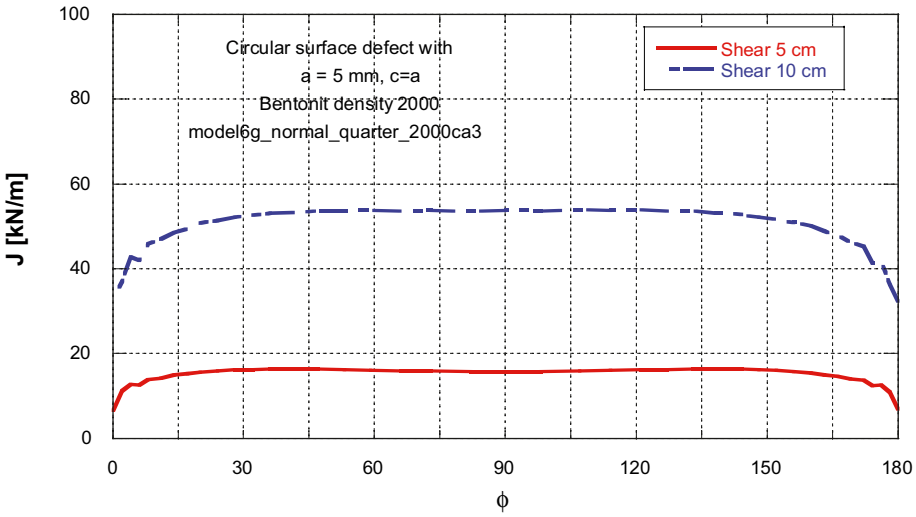

Figure B-5. *J-integral for a semi-circular surface defect plotted along the crack front (a = 5 mm).*

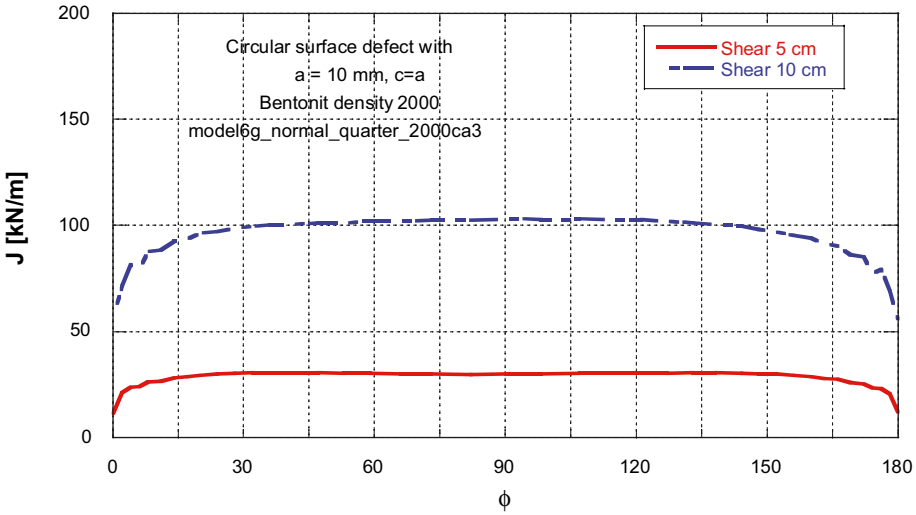

Figure B-6. *J-integral for a semi-circular surface defect plotted along the crack front (a = 10 mm).*

B3 *J*-values for an internal elliptical defect, using a bentonite density of 2,000 kg/m³

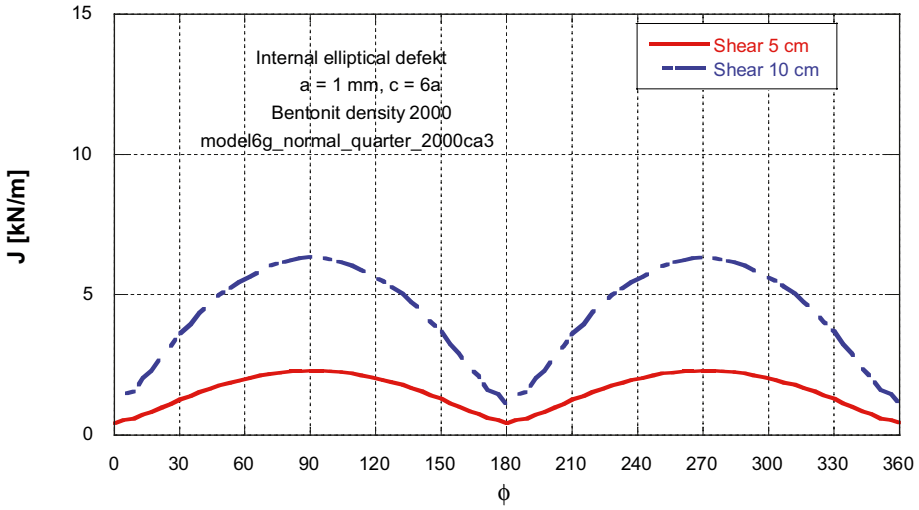

Figure B-7. *J-integral for an internal elliptical defect plotted along the crack front (2a = 1 mm).*

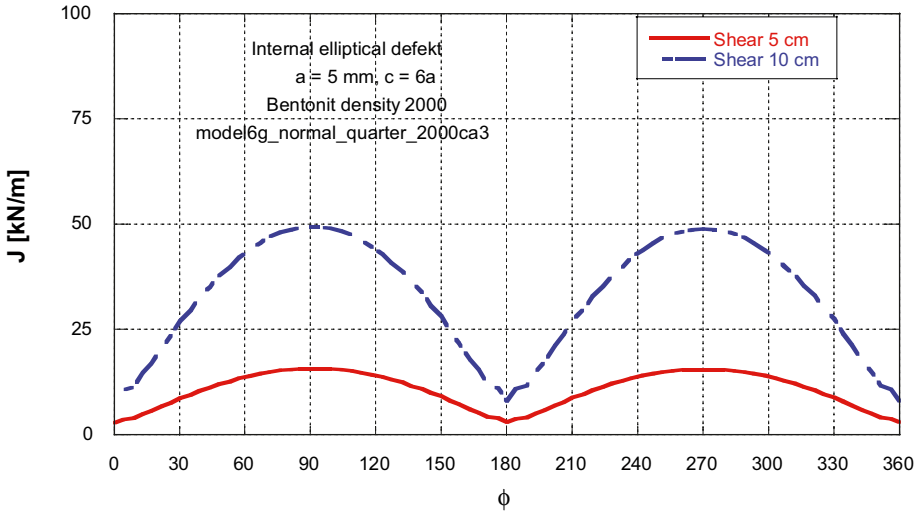

Figure B-8. *J-integral for an internal elliptical defect plotted along the crack front (2a = 5 mm).*

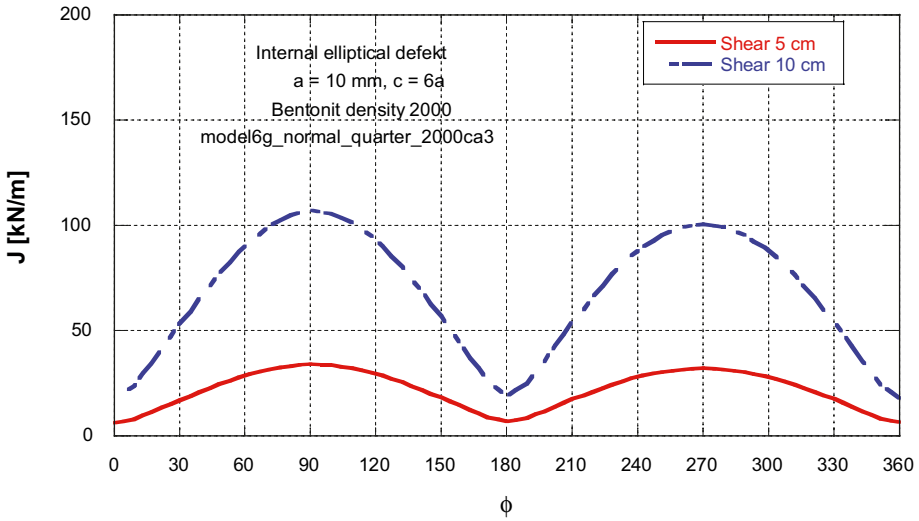

Figure B-9. *J-integral for an internal elliptical defect plotted along the crack front (2a = 10 mm).*

B4 *J*-values for an internal circular defect, using a bentonite density of 2,000 kg/m³

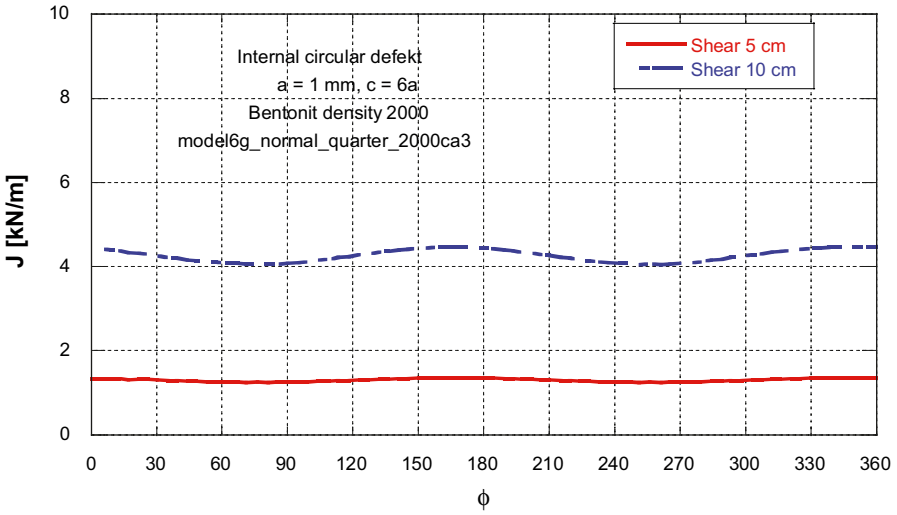

Figure B-10. *J-integral for an internal circular defect plotted along the crack front (2a = 1 mm).*

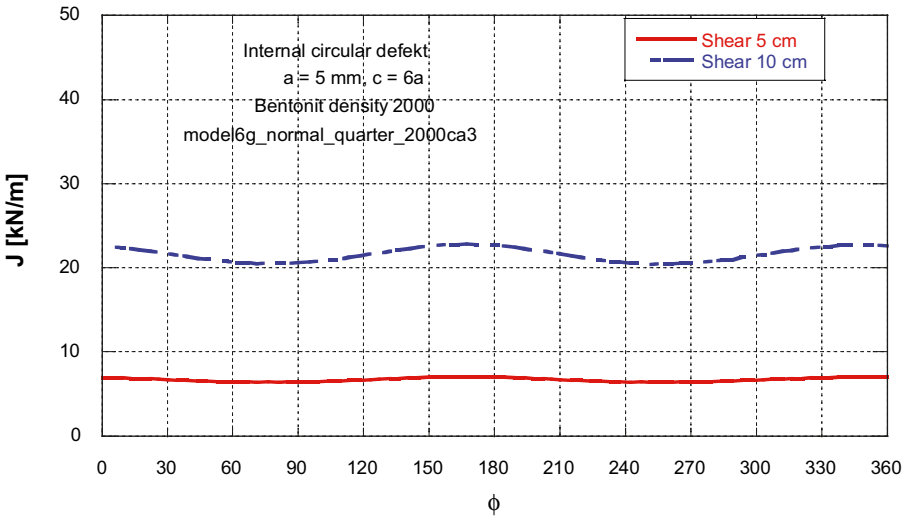

Figure B-11. *J-integral for an internal circular defect plotted along the crack front (2a = 5 mm).*

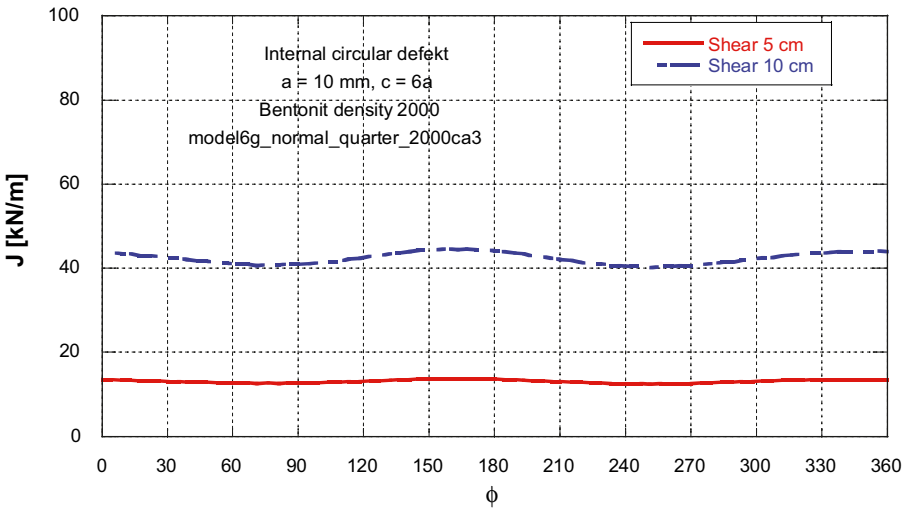

Figure B-12. *J-integral for an internal circular defect plotted along the crack front (2a = 10 mm).*

Appendix C

Calculated *J*-values when using a bentonite density of 2,050 kg/m^3

The results below (for the model *model6g_normal_quarter_2050ca3*) are presented in graphs, using one graph for each type of defect and crack depth. In each graph results along the crack front from two different load magnitudes are plotted (the angle ϕ is defined in Figure 2-5). Each load magnitude corresponds to 5 and 10 cm shear of the BWR canister including the bentonite clay.

C1 *J*-values for a semi-elliptical surface defect, using a bentonite density of 2,050 kg/m^3

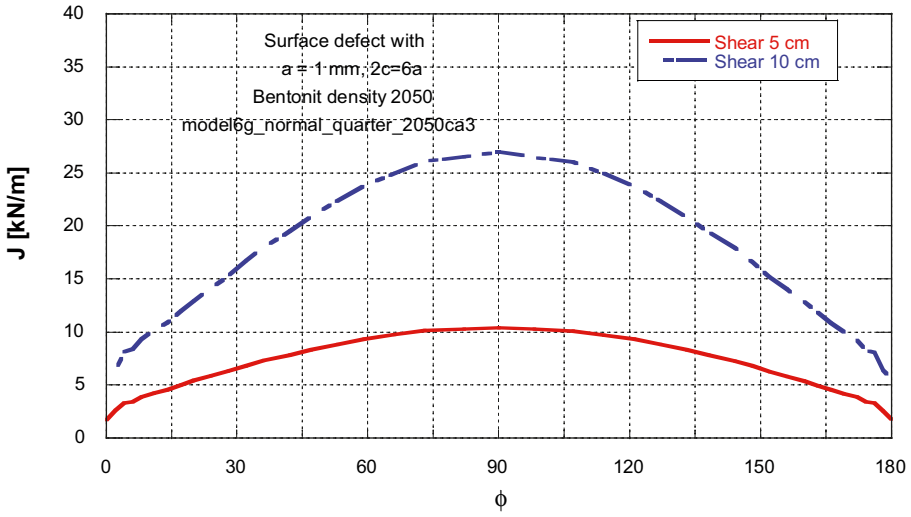

Figure C-1. *J-integral for a semi-elliptical surface defect plotted along the crack front (a = 1 mm).*

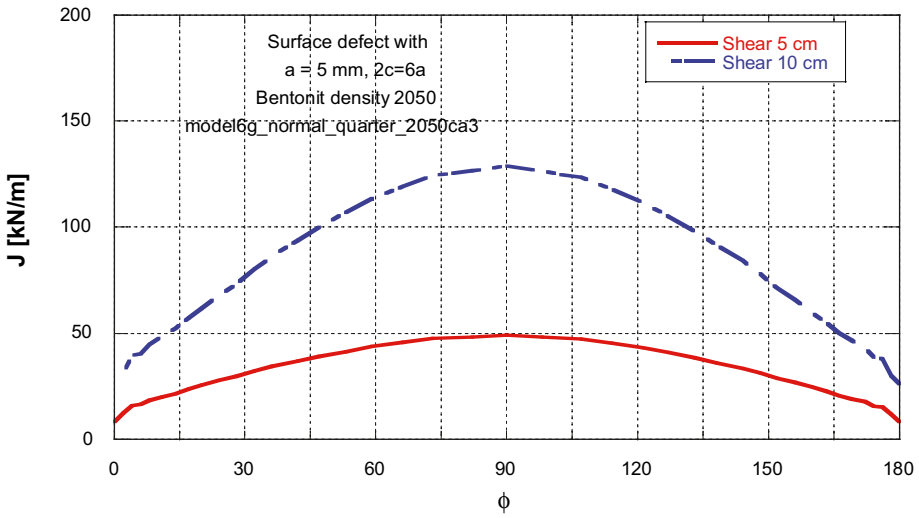

Figure C-2. *J-integral for a semi-elliptical surface defect plotted along the crack front (a = 5 mm).*

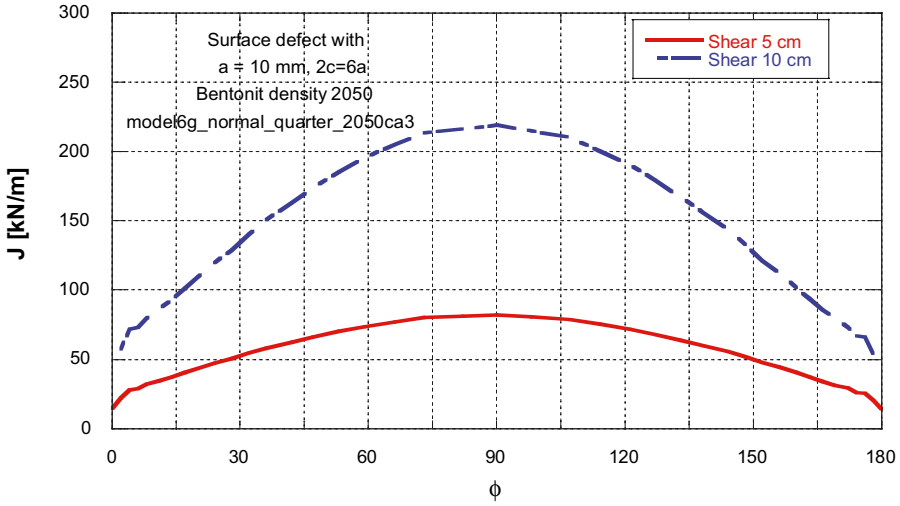

Figure C-3. *J-integral for a semi-elliptical surface defect plotted along the crack front (a = 10 mm).*

C2 *J*-values for a semi-circular surface defect, using a bentonite density of 2,050 kg/m³

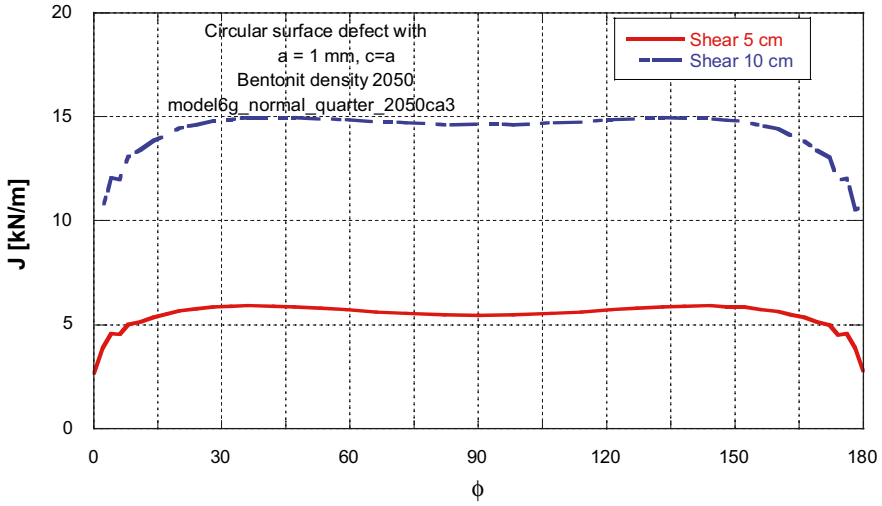

Figure C-4. *J-integral for a semi-circular surface defect plotted along the crack front (a = 1 mm).*

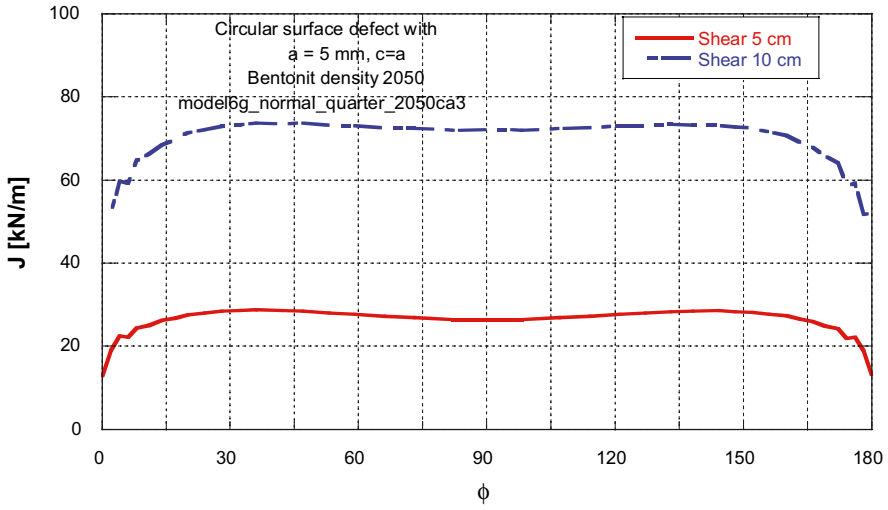

Figure C-5. *J-integral for a semi-circular surface defect plotted along the crack front (a = 5 mm).*

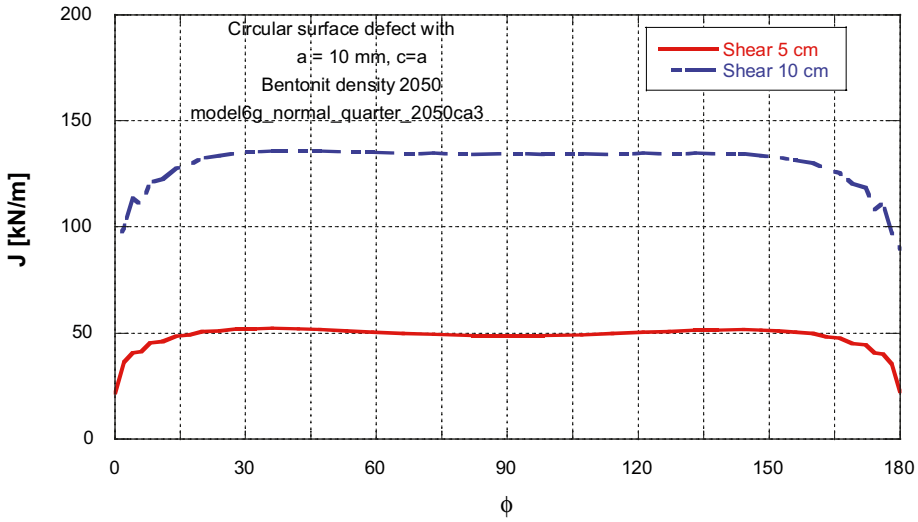

Figure C-6. *J-integral for a semi-circular surface defect plotted along the crack front (a = 10 mm).*

C3 *J*-values for an internal elliptical defect, using a bentonite density of 2,050 kg/m³

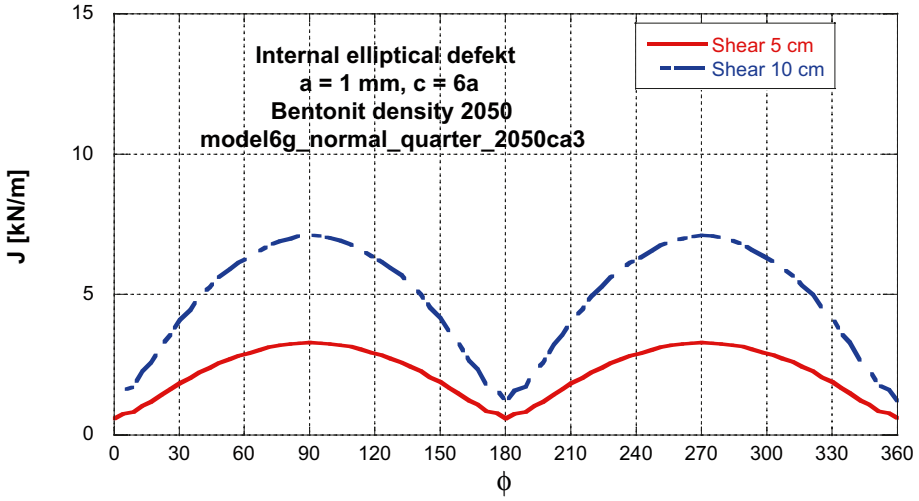

Figure C-7. *J-integral for an internal elliptical defect plotted along the crack front (2a = 1 mm).*

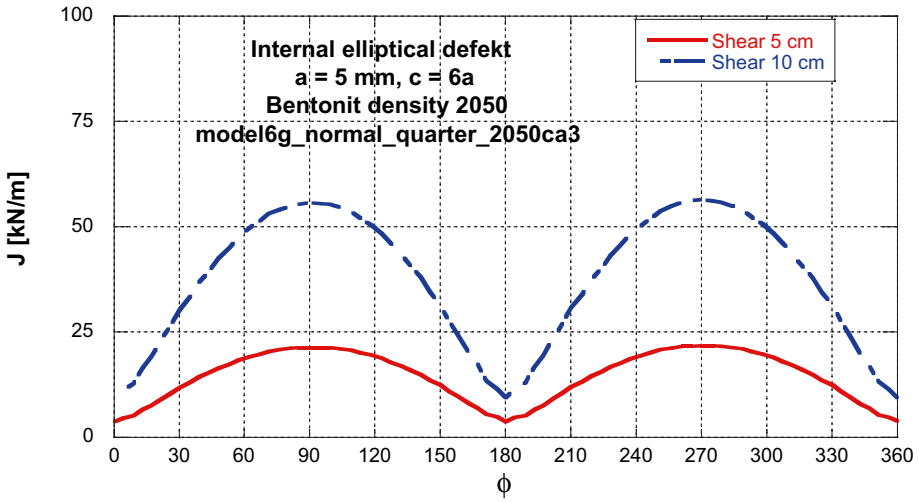

Figure C-8. *J-integral for an internal elliptical defect plotted along the crack front (2a = 5 mm).*

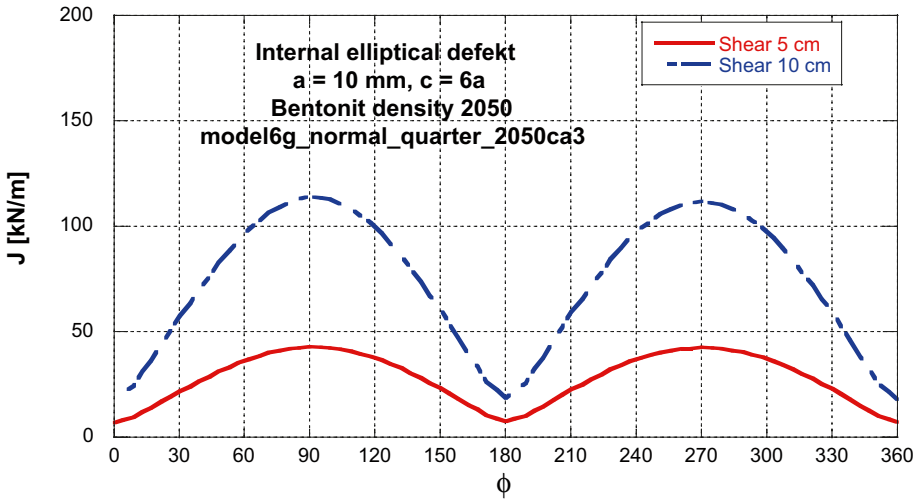

Figure C-9. *J-integral for an internal elliptical defect plotted along the crack front (2a = 10 mm).*

C4 *J*-values for an internal circular defect, using a bentonite density of 2,050 kg/m³

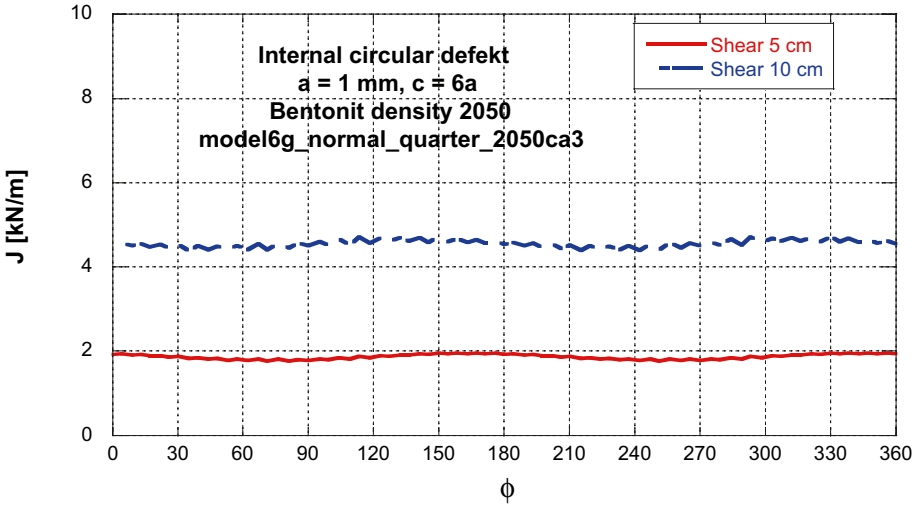

Figure C-10. *J-integral for an internal circular defect plotted along the crack front (2a = 1 mm).*

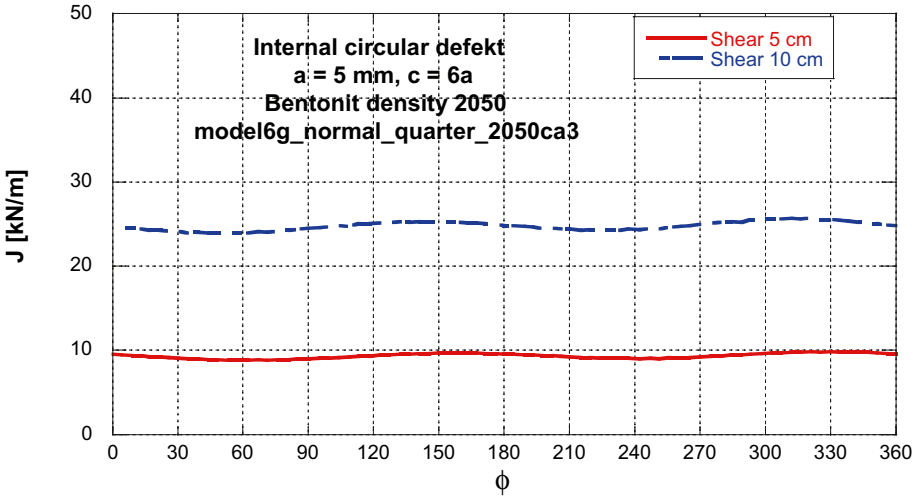

Figure C-11. *J-integral for an internal circular defect plotted along the crack front (2a = 5 mm).*

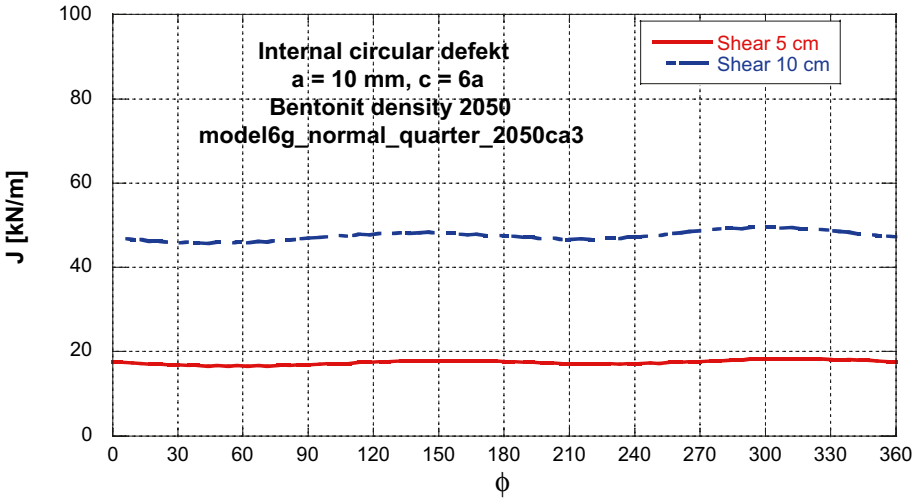

Figure C-12. *J-integral for an internal circular defect plotted along the crack front (2a = 10 mm).*